frontiers in Earth Science

ORIGINAL RESEARCH
published: 03 January 2022
doi: 10.3389/feart.2021.790526

Deciphering the Late Paleozoic–Cenozoic Tectonic History of the Inner Central Andes Forearc: An Update From the Salar de Punta Negra Basin of Northern Chile

Fernando Martínez[1], Mauricio Parra[2], Rodrigo Gonzalez[3], Cristopher López[3], Patiño Ana[2], Belén Muñoz[4], Francisca Robledo[5], Edward R. Sobel[6] and Johannes Glodny[7]*

[1]Carrera de Geología, Facultad de Ingeniería, Universidad Andres Bello, Campus República, Santiago, Chile, [2]Institute of Geosciences, University of Sao Paulo, Sao Paulo, Brazil, [3]Departamento de Ciencias Geológicas, FICG, Universidad Católica del Norte, Antofagasta, Chile, [4]Departamento de Geología, FCFM, Universidad de Chile, Santiago, Chile, [5]School of Geosciences, University of Aberdeen, Aberdeen, United Kingdom, [6]Institute of Geosciences, University of Potsdam, Potsdam, Germany, [7]German Research Center for Geosciences (GFZ), Potsdam, Germany

We integrated new and existing geological, geochronological, thermochronological, and two-dimensional (2D) seismic data from the Salar de Punta Negra Basin to define the Late Paleozoic–Cenozoic tectonic evolution of the inner Andean forearc of northern Chile more precisely. Our results indicate that this region experienced early Late Paleozoic–Mesozoic crustal extension, creating several basement half-graben structures bounded by east- and west-dipping master faults. These extensional basins were filled by Upper Permian to Jurassic volcanic and sedimentary (continental and marine) syn-rift deposits. The genesis of these structures is related to the early breakup of the western Gondwana continent and the development of the large Tarapacá Basin in northern Chile and southern Perú. Subsequently, Late Cretaceous to Paleocene contraction occurred, which led to the tectonic inversion of the pre-existing rift system and the uplift of the Paleozoic–Mesozoic syn-rift deposits. Seismic data show that Upper Cretaceous and Paleocene synorogenic deposits accumulated along and over inversion anticlines, recording the initial contraction and marking the change from an extensional to a contractional tectonic setting. During the final episodes of basin inversion, crustal shortening was accommodated by the Eocene to recent basement reverse faulting accompanied by the rapid exhumation of basement pre-rift blocks, which served as the principal sources for the sediments that filled the pre-Andean basins during the Late Cenozoic. Finally, the exhumed basement pre-rift blocks and the reverse faults compartmentalized the contractional intermontane basins, which constitute the main low topographic relief of the inner forearc of northern Chile.

Keywords: central andes, salar de punta negra basin, basin inversion, late paleozoic-cenozoic tectonic, contractional tectonics

OPEN ACCESS

Edited by:
Gang Rao,
Southwest Petroleum University, China

Reviewed by:
Ruth Soto,
Instituto Geológico y Minero de España (IGME), Spain
Nicholas Perez,
Texas A&M University, United States
Yiquan Li,
Nanjing University, China

****Correspondence:***
Fernando Martínez
fernando.martinez@unab.cl

Specialty section:
This article was submitted to Structural Geology and Tectonics, a section of the journal Frontiers in Earth Science

Received: *06 October 2021*
Accepted: *29 November 2021*
Published: *03 January 2022*

Citation:
Martínez F, Parra M, Gonzalez R, López C, Ana P, Muñoz B, Robledo F, Sobel ER and Glodny J (2022) Deciphering the Late Paleozoic–Cenozoic Tectonic History of the Inner Central Andes Forearc: An Update From the Salar de Punta Negra Basin of Northern Chile. Front. Earth Sci. 9:790526. doi: 10.3389/feart.2021.790526

1 INTRODUCTION

The inner forearc of the Central Andes comprises a series of intermontane basins located between the Domeyko Cordillera (or Chilean Precordillera) and the volcanic arc (**Figure 1**) that extends for approximately 450 km between 22° and 26°30S latitude. These correspond to the Salar de Atacama, Salar de Punta Negra, and Salar de PedernalesBasins (**Figure 1**). All these basins are isolated topographic lows established on a plateau elevated to 2.5 km above mean sea level and covered by a mix of salt flats and recent volcanic products, which hide their internal tectonic and stratigraphic architecture. For many years, numerous studies developed in the region (Muñoz et al., 2002; Pananont et al., 2004; Mpodozis et al., 2005; Arriagada et al., 2006; Bascuñán et al., 2016, Bascuñán et al., 2019; Martínez et al., 2018; Henriquez et al., 2018, among others) have focused on understanding the evolution of the Andean forearc using the Salar de Atacama Basin as a natural laboratory. This is due to its easy access and the good natural outcrops that occur. In contrast, other modern and smaller depocenters (e.g., the Salar de Punta Negra and Salar de Pedernales Basins) with excellent records of Paleozoic to recent geological units have received little attention, thus generating a gap in the full geological knowledge of the Andean forearc.

Previous works conducted in the Salar de Atacama Basin have commonly been supported by field, geochronologic, paleomagnetic, and two-dimensional (2D) seismic data (Jordan et al., 2002; Pananont et al., 2004; Mpodozis et al., 2005; Arriagada et al., 2006; Jordan et al., 2007; Bascuñán et al., 2016; Rubilar et al., 2017; Bascuñán et al., 2019; López et al., 2019). These data interpreted the structure of the inner Central Andes forearc to result from the superimposed extensional and contractional tectonic regimes affecting the western continental margin from the Late Paleozoic, which were related to variations in plate kinematics (Pacific and South American plates). Although some of the abovementioned works argued that the region was affected by the Early Mesozoic generalized lithospheric extension associated with the breakup of western Gondwana (Mpodozis et al., 2005; Mpodozis and andRamos, 2008; Espinoza et al., 2018), clear pieces of evidence have not been documented; therefore, the styles, mechanisms, and age of this deformation have not been completely well constrained, as much of the field data used as evidence are still questioned. In addition, a long debate (lasting more than 20 years) has existed for the Cenozoic tectonic evolution of the region and two end-member interpretations are frequently invoked. One interpretation suggests that during the Cenozoic, the Andean forearc was preferentially compressed and regional-scale thrust fault systems and flexural basins were developed (Muñoz et al., 2002; Arriagada et al., 2006; Bascuñán et al., 2016; Henriquez et al., 2018; Bascuñán et al., 2019). A second interpretation considers a mix of contractional–extensional–contractional tectonic alternations during the Cenozoic, thus allowing kilometric-scale basement faults to be repeatedly reactivated as reverse and/or normal faults (Flint et al., 1993; Pananont et al., 2004; Jordan et al., 2007; Rubilar et al., 2017). Each interpretation requires different mechanisms to explain the building of the western Central Andes, and these are commonly used to constrain the models of exhumation, erosion, and shortening as well as to explore mineral resources. To contribute to this large debate, we present a new and updated tectonic framework for the Late Paleozoic–Cenozoic tectonic evolution of the inner Central Andes forearc but with a special focus on the Salar de Punta Negra Basin of northern Chile (**Figures 1**, **2**).

In this work, we present an integrated study based on 1) an analysis of stratigraphic cross-cutting relationships observed at the northern and easternmost part of the basins, and the neigboring region of the Domeyko Cordillera (Sierra de Varas sector), 2) a reinterpretation of 2D seismic profiles, 3) previous U–Pb ages of synorogenic deposits, 4) the first sequential restoration of regional 2D cross sections made for this basin, and 5) a new apatite fission track (AFT) and (U–Th–Sm)/He analyses. We provide a new interpretation for the tectonic history of the inner forearc of the Central Andes, which could be used to reconstruct the western slope of the orogen. The results will help to understand the mechanisms and styles of deformation experienced by contractional forearc settings preceded by rifting and crustal extension. These can be used as a reference to compare similar tectonic scenarios both in the Andes and in other provinces worldwide.

2 GEOLOGICAL SETTING

Subduction orogenesis since the Late Cretaceous (Horton, 2018) has shaped the Central Andes, especially its westernmost part in northern Chile. This process has led to the development of a magmatic arc as well as several intermontane basins in the inner forearc region (**Figure 1**) where the Salar de Punta Negra Basin is located. The Paleozoic to Cenozoic geological units that internally compose this basin, and the youngest Miocene to Pliocene volcanic products covering the area are well exposed along the western and eastern flanks coinciding with the eastern Domeyko Cordillera (or Chilean Precordillera) and the western section of the volcanic arc (**Figure 2**).

The basement rocks of the basin are represented by Devonian sedimentary successions and Carboniferous to Lower Permian crystalline granitic rocks, which are preferably recognized along the core of the Domeyko Cordillera, at the Sierra de Almeida, and southern Cordón de Lila (**Figure 2**). The Devonian unitscrop out in the central section of the Sierra de Almeida (**Figure 3**). Here, these consist of 600 m of light-gray quartzites with intercalated conglomerates, sandstones, and fossiliferous shales assigned to the Zorritas Formation (Cecioni and Frutos, 1975; Solari et al., 2017; **Figure 4**). These rocks have been attributed to shallow marine deposits accumulated in an ancient Paleozoic backarc basin, which was previously established in the present-day position of the Domeyko Cordillera (Bahlburg and Breitkreuz, 1991; Rubinstein et al., 1997). Kilometric-scale Carboniferous to Lowe Permian granitic bodies (granodiorites and monzogranites) are well exposed at the Sierra de Varas sector of the Domeyko Cordillera, and also in the central and southern part of the Sierra de Almeida (**Figure 3**), where these are grouped into the Imilac Complex, a large basement block made of granites that intrude

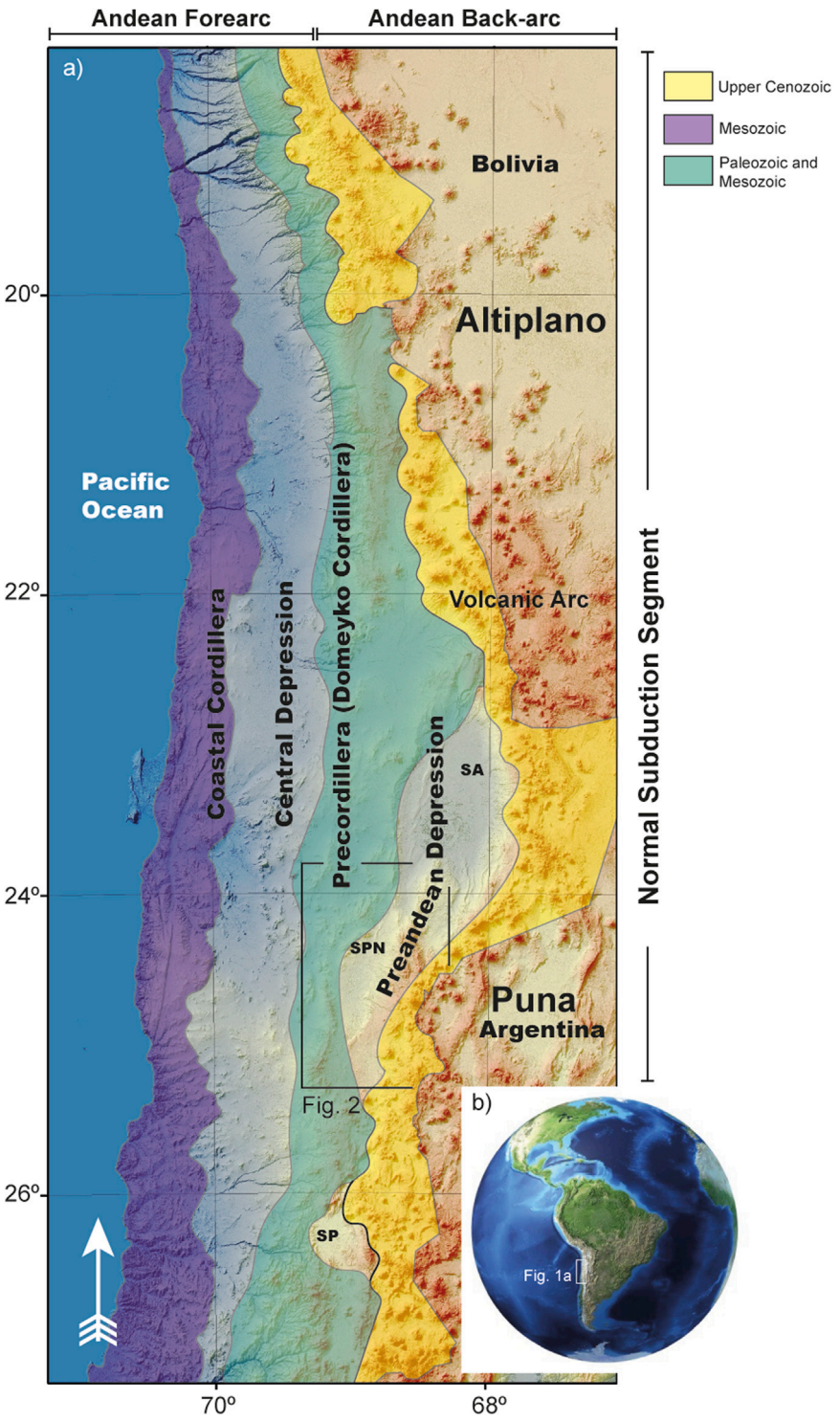

FIGURE 1 | Continental-scale image of the Central Andes of South America showing the distribution of the main tectonic provinces and cordilleras in northern Chile, as well as the location of the study region.

the Devonian Zorritas Formation (Cecioni and Frutos, 1975; Gardeweg et al., 1994; Solari et al., 2017).

The Paleozoic granitic rocks exposed in the Domeyko Cordillera and the Sierra de Almeida (Imilac Complex) as well as the Devonian Zorritas Formation are partially covered by a coeval volcanic succession of stratified laves, rhyolites, and breccias defined as La Tabla Formation (**Figures 3**, **4**). This unit is locally affected by metric-scale normal faults

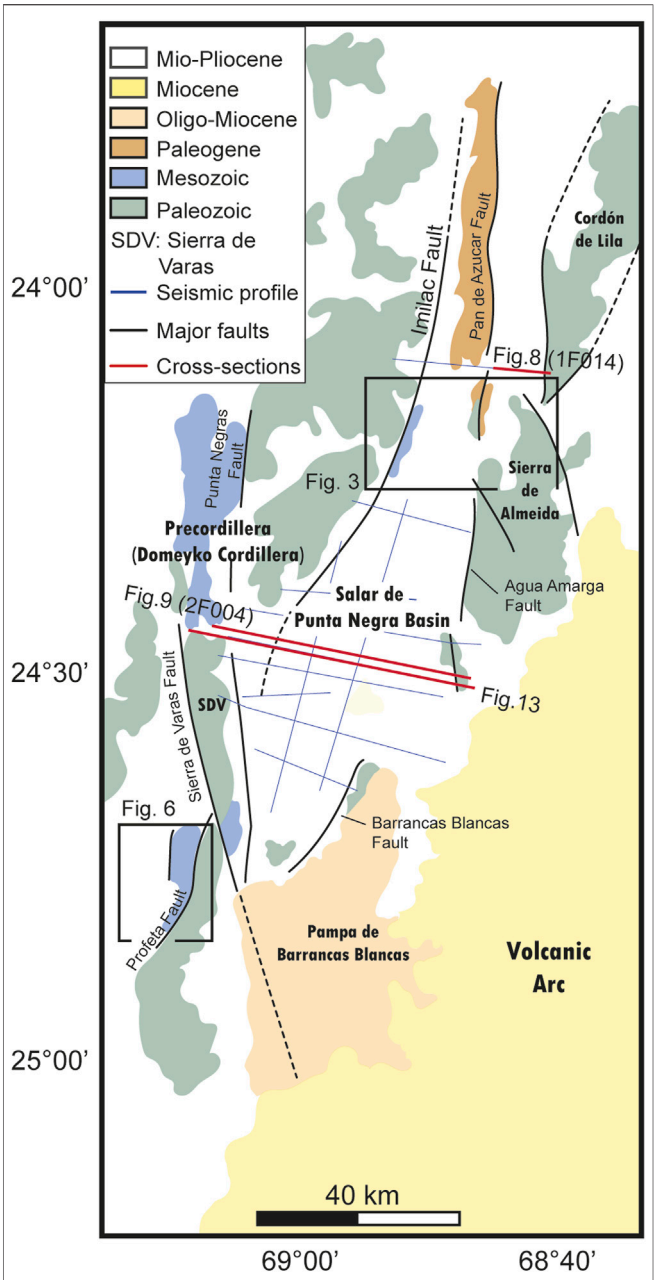

FIGURE 2 | Simplified regional-scale geological map showing the distribution of the first-order units and structures exposed in the Salar de Punta Negra Basin and neighboring regions indicating the location of the2D seismic grid available in the study area, and the2D seismic profiles presented in this work (red lines).

(Marinovic et al., 1995; Niemeyer et al., 1997; Solari et al., 2017; Martínez et al., 2018). A recent analysis of regional 2D seismic profiles along the basin has identified a wedge shape for this formation associated with a syn-rift stratigraphic sequence (Martínez et al., 2018; **Figure 4**). Triassic and Jurassic rocks are preferentially exposed on the Sierra de Varas sector in the Domeyko Cordillera (**Figure 2**) and the westernmost part of the Salar de Punta Negra Basin (**Figure 3**), however, in the last only crop out Triassic successions. The basal units consist of Upper Triassic successions formed by nearly 800 m of intercalated lavas, red conglomerates, and red sandstones defined as the Sierra de Varas Formation and/or Pular Formation (González et al., 2015; Solari et al., 2017; Espinoza et al., 2018; **Figure 4**). This unit is unconformably covered by Jurassic marine sedimentary deposits (**Figure 4**) of variable thicknesses, which usually exhibit a wedge shape with a maximum thickness of nearly 1,500 m, and is composed of gray–black fossiliferous shales, calcareous sandstones, limestones, and minor calcareous conglomerates assigned to the El Profeta Formation (Chong, 1973; Amilibia et al., 2008; González et al., 2015, Espinoza et al., 2018; **Figure 4**). Recent works based on the comparative analysis of field data with 2D seismic profiles have evidenced that both the Pular and El Profeta formations correspond to syn-rift successions accumulated on domino-style and half-graben basement structures (Espinoza et al., 2018; Martínez et al., 2018; López et al., 2019).

The Upper Cretaceous–Cenozoic record comprises two units: an Upper Cretaceous–Paleocene stratigraphic section that crops out in the northeastern part of the Sierra de Almeida and on the Cordón de Pan de Azucar (**Figure 3A**). The basal units of this section (**Figure 4**) comprise sedimentary and volcanic deposits that include nearly 800 m of red polymictic conglomerates, sedimentary breccias, sandstones, and shales (**Figure 5A**). A recent work (Martínez et al., 2019) has reported detrital zircon U–Pb ages with youngest populations that range from 70 to 53 Ma. Commonly, the oldest ages among them are reported in the basal red sedimentary rocks identified as the Pajonales Formation (Solari et al., 2017; **Figure 5A**), whereas the youngest occur in the conglomerates and sandstones exposed at the Cordón de Pan de Azucar and related to the Naranja Formation (Arriagada et al., 2006; **Figures 5B,C**). In the field, both successions internally exhibit apparent contractional growth strata within synclines and exhibit on-lap terminations on their limbs (**Figure 5B**), thus indicating that these were accumulated during tectonic contractions; however, this stratigraphic pattern is better observed in seismic profiles (Arriagada et al., 2006; Martínez et al., 2019).

The second unit corresponds to the Upper Paleogene–Neogene rocks cropping out in the eastern section of the Sierra de Almeida (**Figure 3**) and in the south-central part of the basin (Solari et al., 2017). It comprisesthe Upper Oligocene–Lower Miocene brown conglomerates, sandstones, and tuffs defined as the Pampa de Mulas Formation as well as Upper Miocene–Pleistocene unconsolidated sandstones, gravel, and ignimbrites. Previous analyses of2D seismic profiles identified important variations in the thicknesses of the Upper Oligocene and Upper Miocene successions across contractional folds, with thinner accumulations over the hinge of anticlines and thicker on the limbs, indicating an accumulation concurrent with the growth of the contractional structures (Martínez et al., 2018; 2019). Finally, the stratigraphic record culminates upward with recent gypsum beds and volcanic flows (Gardeweg et al., 1994; Marinovic et al., 1995; Soto et al., 2005).

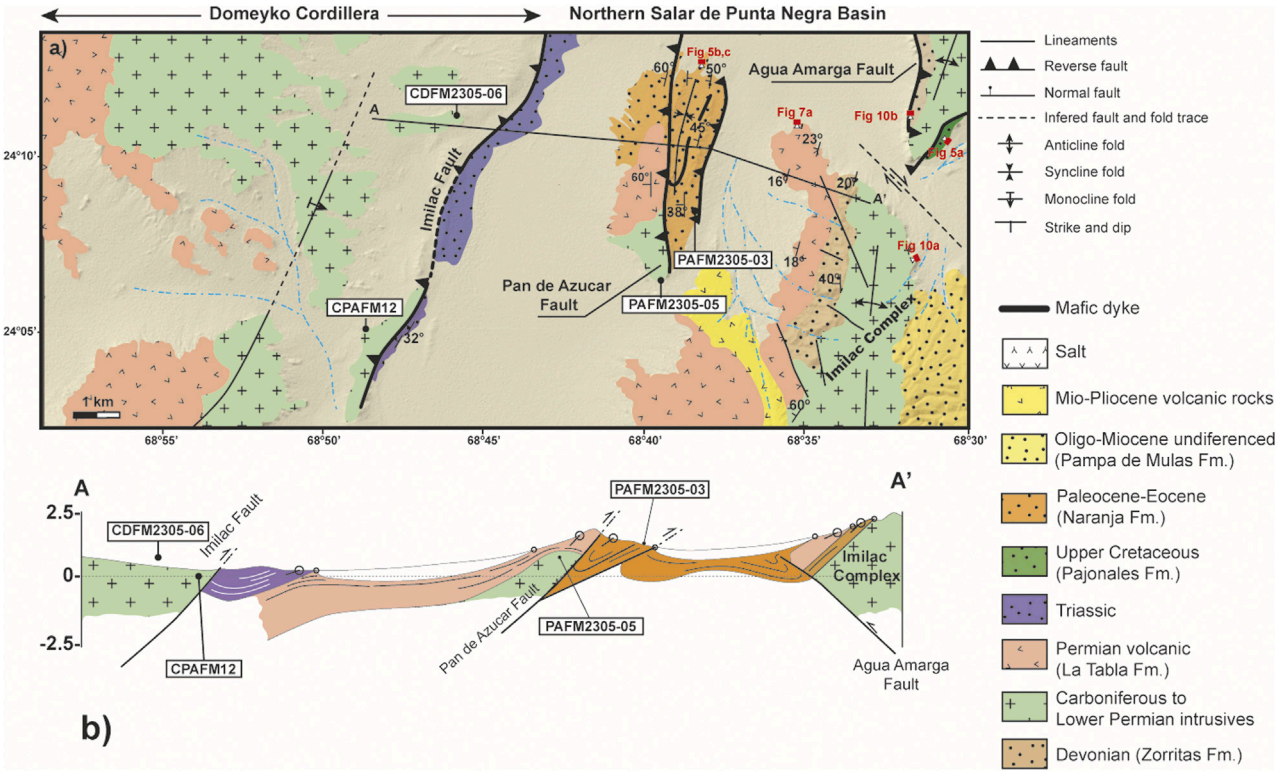

FIGURE 3 | (A) Geological map of the northern and central sections of the Salar de Punta Negra Basin and the eastern Domeyko Cordillera showing the distribution of the main basement-involved reverse faults and the Paleozoic to recent geological units exposed in the region, as well as the location of the rock samples collected in this study, **(B)** generalized stratigraphic column showing the vertical relationships between the different geological units recognized in the field, and **(C)** structural cross-section A–A′, along which the geometry of the main faults and folds are represented.

3 METHODOLOGY

The reconstruction of the basin architecture was based on geological mapping integration, reinterpretation of2 D seismic profiles, low-temperature thermochronology, and the restoration of a regional-scale structural cross section, each of which are described below.

3.1 Geological Mapping Integration¶

In two simplified geological maps (**Figures 3**, **6**), we integrated previous (González et al., 2015; Solari et al., 2017) and new stratigraphic and structural data (cross-cutting relationships along regional faults and folds, recognition of structural styles, and dip domains) of the northern and central parts of the Salar de Punta Negra and Sierra de Varas sectors in the Domeyko Cordillera. Both areas were selected because along these the Paleozoic to Cenozoic record is well preserved, thus having a good constrain of the stratigraphic units that they allow to reconstruct the architecture of the basin. The new structural and stratigraphic dataconsist of strike, dip, stratigraphic thickness measurements, inspection of the geometry and orientation of regional- and mesoscopic-scale faults and folds, type of geological contacts between stratigraphic units. The previous geological data consists of geochronological data (mainly U–Pb ages) determined for igneous and sedimentary rocks, and also we used the distribution of the stratified and igneous rocks to construct local cross-sections. The data were taken on outcrops well exposed along the main creeks and roads. The geological mapping was supported by the visualization of Landsat images at different scales (1:25,000, 1:50,000, and 1:100,000). We also used satellite images obtained from the Google Earth Pro platform to examine places that aredifficult to access.

3.2 Two-Dimensionalseismic and Structural Interpretation

The seismic data consist of a2D seismic grid of approximately 2,300 km^2 composed of N–S and WNW–ENE seismic profiles, which were provided by Empresa Nacional del Petróleo (ENAP) Sipetrol (**Figures 2**, **3A**). To improve the previous seismic and structural interpretations of these data, this study increased the seismic amplitudes of those seismic reflectors related to angular unconformities and fault planes to obtain a cleaner image of these and refine the location of the tops and bottoms of the main tectonic sequences, the geometry of the faults and folds, and volcanic products. We choose two seismic profiles (1F014 and 2F004) located in the northern and central sections of the Salar de Punta Negra Basin (**Figures 2**, **3A**) because these profiles exhibit a moderate-to-good quality. These were initially filtered and then migrated using two-way-travel time (TWT) to eliminate the

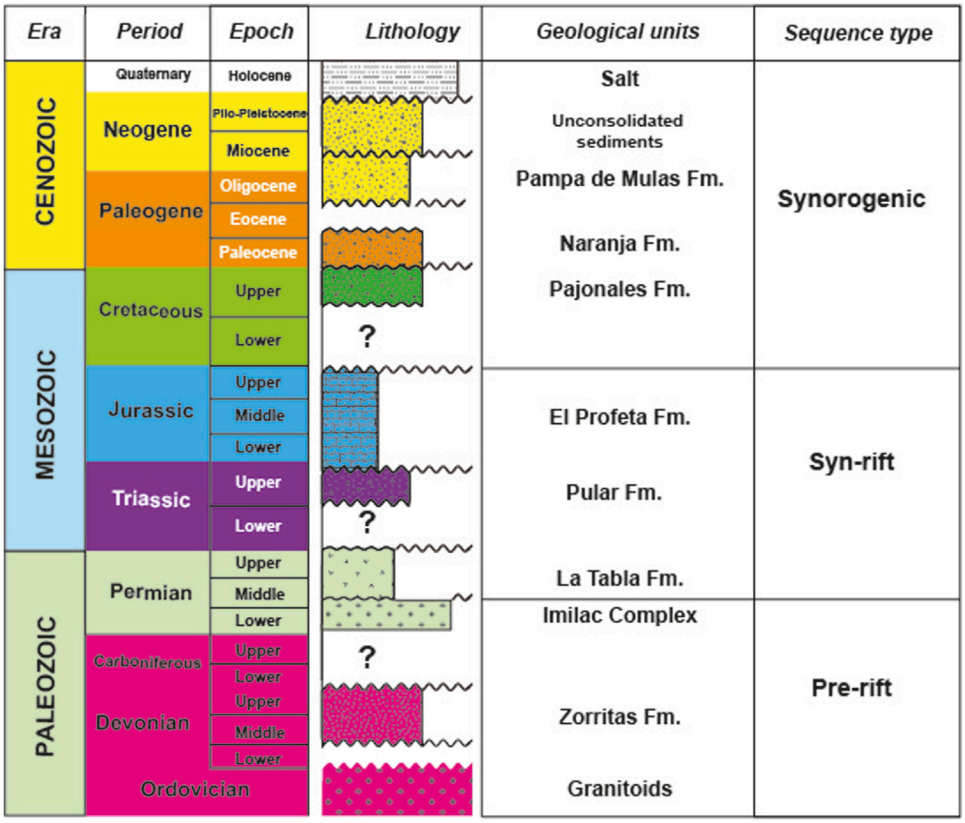

FIGURE 4 | Stratigraphic template showing the main geological units recognized on the surface along the Salar de Punta Negra Basin and their tectonic interpretation. The undulating lines indicate regional-scale unconformities (modified from Martínez et al., 2019).

seismic pitfalls (and/or artifacts) that prevent correct interpretation of the data. Considering that this study lacks an exploratory purpose as well as key geophysical information, such as density, velocity, and check shot logs to develop time–depth calibration, the seismic data were interpreted using TWT.

The top of the main geological units was constrained by surface data. Generally, geologic contacts are exposed well at the surface; therefore, their projection at depth in the first 3 seconds is quite reliable. Several contacts define angular unconformities with a high seismic amplitude that can be followed easily along the entire 2D seismic grid because they are marked by top-lap and/or on-lap terminations against the seismic reflectors, whereas the crystalline basement rocks (granitoids) are characterized by a chaotic and transparent seismic signal with low internal impedance contrasts. To understand the stratigraphic record under the basin, we correlated the tectonic sequences and unconformities observed with those previously interpreted under the Salar de Atacama Basin located 18 km to the north. We used the following four criteria to interpret the faults and folds:

(1) Identification of abrupt lateral terminations (cutoffs) and/or an offset of seismic reflectors
(2) Identification of fault-plane reflections
(3) Abrupt termination of anticline and syncline folds
(4) Abrupt lateral contact between stratified and chaotic seismic reflectors (see Martínez et al., 2020a, b for details)

We used the Andino and StructureSolver software packages to visualize and interpret the digital seismic data.

3.3 Construction a Retrodeformable Cross Section

We constructed a regional balanced cross section from the interpretation of the 2D seismic profile 2F004 (**Figure 2**), which shows the complete structure of the basin projecting from the eastern Domeyko Cordillera to the western volcanic arc. This section was elaborated by projecting to the subsurface the first-order faults and folds, the dips of the beds, and the contact between geological units, as presented in **Figure 3A**. The contacts between the geological units were correlated with the top and/or button of the different tectonic sequences previously interpreted in the seismic profile. Further, we used the stratigraphic thickness reported both in the literature (González et al., 2015; Solari et al., 2017) and estimated for us in the field to construct the stratigraphic packages following the structure identified in the 2F004 seismic profile.

To determine the magnitude and changes in the entire basin related to shortening and extension and to know the initial shape

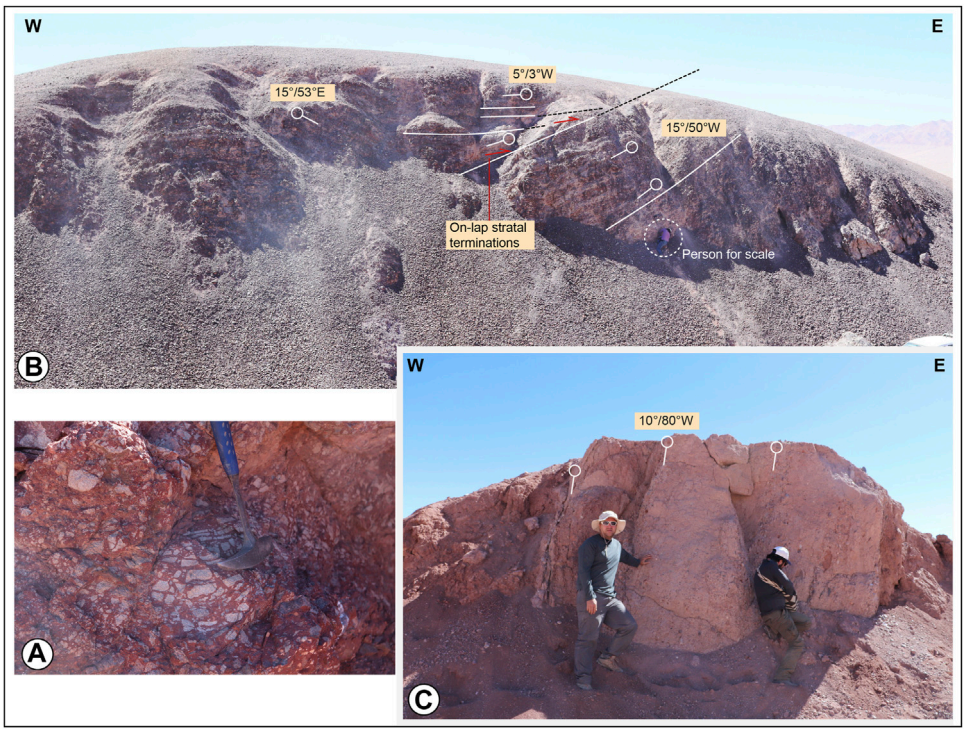

FIGURE 5 | (A) Upper Cretaceous sedimentary breccias of the Pajonales Formation exposed along the Sierra de Almeida, **(B)** growth strata and on-lap stratal terminations identified in the core of a syncline fold along the eastern Cordón de Pan de Azucar sector, and **(C)** intercalation of Paleocene (Naranja Formation) red sandstones and conglomerates on the limb of a syncline exposed in the Cordón de Pan de Azucar in the northern part of the Salar de Punta Negra Basin (see **Figure 3A** for location of the photographs).

of this, the balanced cross section was sequentially retrodeformed. The retrodeformation was developed assuming the conservation of area before and after deformation as well as the conservation of bed length, which usually is represented by the top or bottom of the stratigraphic beds. The balanced cross section was sequentially restored in five steps, thus showing the progressive growth of the contractional structures from the Late Cretaceous to recent period, and their early extensional deformation from the Permian to the Jurassic. This allowed us to understand some relevant aspects, such as the initial configuration of the rift-related structures (also called pre-Andean structures), the initial stratigraphic architecture of the syn-rift deposits, and how the contraction of the basin occurred. The restoration was achieved using the structural component module of the StructureSolver software (www.structuresolver.com) by applying the simple-shear and flexural-slip algorithms, thus allowing the unfolding and reversing of the individual blocks bounded by faults, and them we tested this using the Andino software (www.andino3.com.ar) by some specifically forward models of the restored faults.

3.4 Low-Temperature Thermochronology

We applied apatite fission-track (AFT) and apatite (U–Th–Sm)/He (AHe) analyses and thermal modeling to characterize the exhumation patterns of the main ranges surrounding the Salar de Punta Negra Basin (**Figure 2**). These low-temperature thermochronologic methods are based on the thermally activated accumulation of radiogenic products within minerals (i.e., the isotope ^{4}He and crystallographic damage caused by fission tracks) that result from the spontaneous decay of radioactive elements such as ^{238}U, ^{235}U, and ^{232}Th (e.g., Reiners and Brandon, 2006). Three samples of Permian granitoids from the eastern Domeyko Cordillera, Pan de Azucar sector, and western Sierra de Almeida were analyzed by the AFT (samples CDFM2305-06, PAFM2305-05, and CPAFM12; **Figure 3**; see description in **Section 2**) and one sample (PAFM2305-03) for AHe.

The apatites were concentrated by conventional heavy-liquid and magnetic-separation procedures. Individual apatite grains were mounted in epoxy resin and etched in 5.5-M HNO_3 at 20°C ± 1°C for 21 s, based on the methods described in Sobel and Seward (2010). For two samples with abundant apatite, a second aliquot was mounted and sent for ^{252}Cf irradiation to enhance the number of confined tracks available for measurement. Analytical procedures followed the external detector method (Gleadow and Duddy, 1981). The samples, assembled with dosimetry glass CN-5 were irradiated in the IEA-R1 research reactor at the Nuclear Research Institute (IPEN) at the University of São Paulo, Brazil, using a neutron fluence of 9 E15 n cm^{-2}. Following irradiation, induced tracks were etched with 40% hydrofluoric acid at 21°C for 45 min. Samples were counted at the Institute of Energy and Environment, University of São Paulo, with 1,250× magnification

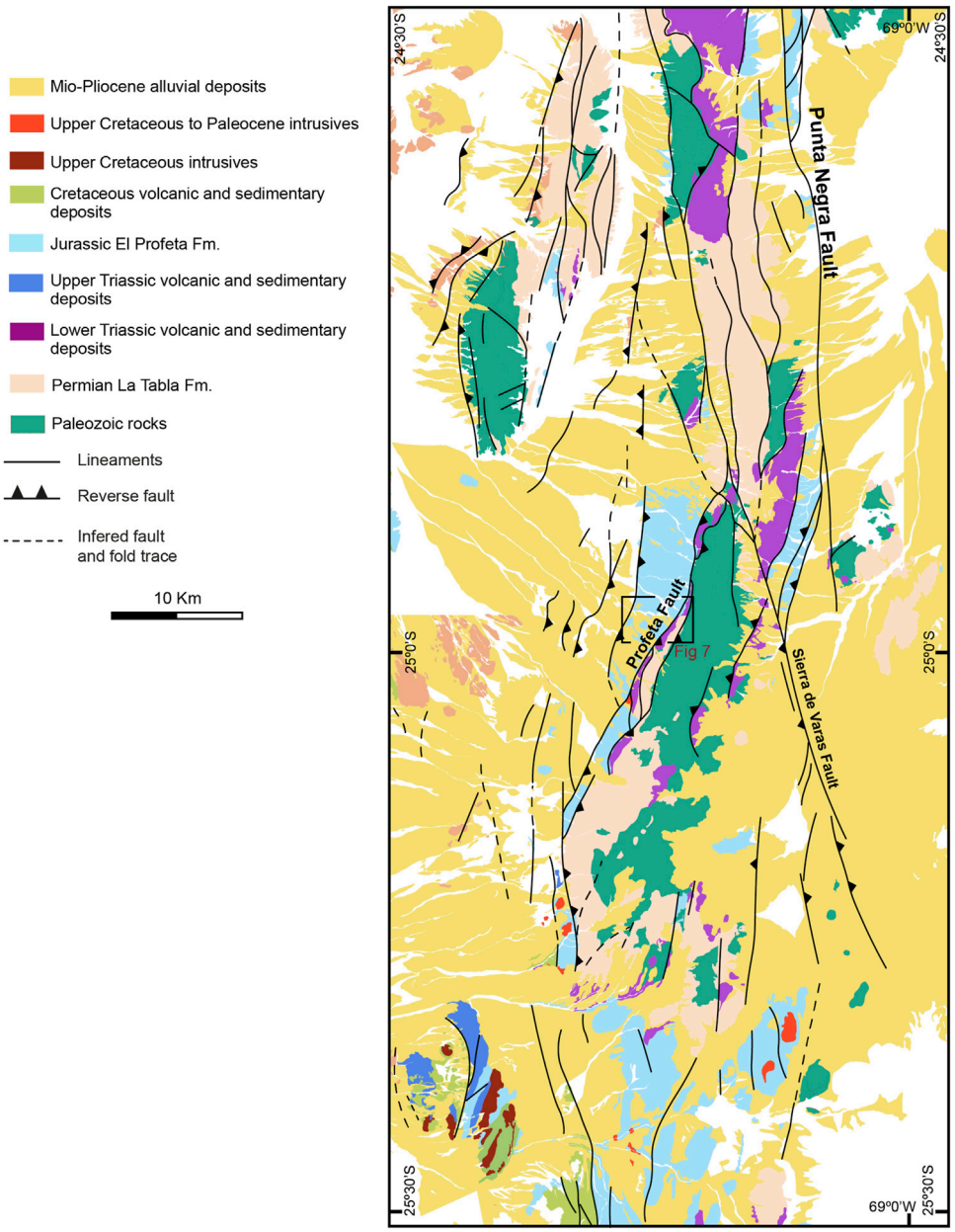

FIGURE 6 | Geological map of the eastern Domeyko Cordillera (modified from González et al., 2015) at the Salar de Punta Negra Basin latitude (see **Figure 2**) showing the distribution of the Paleozoic and Mesozoic (Triassic, Jurassic, and Cretaceous) rocks incorporated in a hybrid (thick and thinskinned) west-verging fold-and-thrust belt. The main geological observations of the Jurassic deposits come from this area.

(dry objective) using an Olympus BX51 microscope with a drawing tube located above a digitizing tablet and a Kinetec^{TM} computer-controlled stage driven by the FTStage 4.0 program (Dumitru, 1993). Age and error calculations were performedusingthe zeta calibration method (Hurford and Green, 1983) witha zeta calibration factor of 350.9 ± 5.5 for CN-5 glass and were reported at the 1σ level (**Table 1**). Confined track lengths, the angle between the confined tracks and the c-crystallographic axis, and the kinetic parameter D_{par} were measured for each grain analyzed (**Table 1**). The belonging of fission-track ages to a single population, i. e, concordance of the age, was assessed with the χ^2 test (Galbraith, 2005), with P (χ2) values > 5% considered as concordant ages.

For the AHe analyses, five individual apatite grains from sample PAFM2305-03 were hand-picked, photographed, and packed in 1-mm Pt tubes using an Olympus SZX16 stereo microscope at the Low-Temperature Thermochronology Lab of the University of São Paulo, following the procedure suggested by Farley (2002). Grain dimensions and the number of terminations were determined to calculate the ejection (Ft)

TABLE 1 | Apatite fission track data determined in this study. The notes under the table are details about the methods used.

Sample number	Long (W)	Lat (S)	Elev.(m)	Lithology	U-Pb agea	# Gr	U (ppm)	Rho-S (NS)[a]	Rho-I (NI)[b]	Rho-D (ND)[c]	P (c2) (%)[d]	FT age (Ma)e	±2 s error	Dpar (mm)	±1 stdev	MTL	±1 stdev	n
PAFM2305-05	7321260	535,207	3,429	Granitoid	280 Ma	22	36.5	8.833 (1,200)	28.840 (3,918)	8.923 (5,141)	11.20	47.7	3.8	2.09	0.24	14.28	2.16	102
PAFM2305-03	7321872	536,945	3,392	Sandstone	50 Ma	20	4.5	2.306 (414)	1.754 (315)	4.515 (2,161)	0.00	93.9	24.5	2.80	0.63	13.00	2.43	11
CDFM2305-06	7329496	524,756	3,023	Granitoid	280 Ma	20	61.3	15.059 (1760)	47.410 (5,541)	8.888 (5,141)	10.60	49.3	5.3	2.05	0.21	13.91	1.34	100
CPA FM12	7320555	518,413	3,116	Granitoid	298–282 Ma	10	18.1	5.078 (270)	14.521 (772)	8.976 (5,141)	9.20	54.8	8.1	2.47	0.54	13.10	1.89	9

[a]*Maximum depositinal age for sedimentary rocks. References are 1: Solari et al. (2020); and 2: Martínez et al. (2020).*

[b]*RhoS and Rho I are the spontaneous and induced tracks density measured, respectively (x 105 tracks/cm2). NS, and NI, are the number of spontaneous and induced tracks counted for estimating RhoS and RhoI, respectively.*

[c]*RhoD is the induced track density measured in the external mica detector attached to CN1 dosimetry glass (x 105 tracks/cm2). ND, is the number of induced tracks counted in the mica for estimating RhoD.*

[d]*(c2) (%) is the chi-square probability (Galbraith, 1981; Green, 1981). Values greater than 5% are considered to pass this test and represent a single population of ages.*

correction factor (Farley et al., 1996). The apatites were degassed with an Alphachron He extraction and analysis system (Australian Scientific Instruments), which was equipped with a Pfeiffer Prisma 200 Quadrupole mass spectrometer (Pfeiffer Group, Germany) at the University of Potsdam, Germany. U, Th, and Sm were analyzed at the German Research Centre for Geosciences (GFZ) at Potsdam by isotope dilution inductively coupled plasma mass spectrometry (ICP-MS). Age calculations followed the procedure of (Meesters and Dunai, 2002). A 2σ uncertainty was reported for all ages. The potential effect of radiation damage on AHe data was assessed by comparing the effective uranium (e [U] = U + 0.235*Th) with individual ages as a proxy for radiation damage, following the model of Flowers et al. (2009).

Thermal history modeling was performed using the QTQt software (Gallagher, 2012) with AFT ages, track lengths, D_{par} measurements, and single-aliquot AHe data. The fission track annealing model of Ketcham et al. (2007) and the radiation-damage annealing model of Flowers et al. (2009) were using for the inversions. Data of two Permian granitoid samples from the hanging-wall block of the Imilac Thrust, located approximately 11 km apart (samples CPAFM-12 and CDFM2305-06) were modeled together. For these Permian granitoid samples, we used a high-temperature constraint (300°C ± 10°C) at the crystallization age derived from available U–Pbage data and a low-temperature constraint of 40°C/Ma ± 15°C/Ma associated with the nearby presence of the overlying Middle–Late Permian volcanic rocks of the La Tabla Fm. For sample PAFM2305-03 from the lower Eocene Naranja Formation, we used a low-temperature constraint using surface temperatures (20°C ± 10°C)at the maximum U–Pb U–Pbdepositional age available of 50 ± 2 Ma (Martínez et al., 2020). We ran 10,000 burn-in and 300,000 postburn-in models and provide the thermal histories and plots of measured vs. modeled ages for comparison.

4 RESULTS

Our field and 2D seismic data show significant geological evidence of at least two main tectonic processes that controlled the Mesozoic–Cenozoic evolution of the basin. The processes correspond to 1) continental crustal extension and 2) tectonic inversion. The data also show stratigraphic evidence of syn-rift and synorogenic deposits hidden under the surface of the basin that facilitate the reconstruction of its tectonic history.

4.1 Evidence of Late Paleozoic–Mesozoic Crustal Extension

On the surface, the main pieces of evidence for tectonic extension are found in the Sierra de Varas sector to the southwest of the Salar de Punta Negra Basin and along the northern section of the Sierra de Almeida (**Figure 2**). At Sierra de Varas (**Figure 6**), specifically at the footwall of the El Profeta fault, a serie of mesoscopic normal faults bounded tilted blocks are well recognized (**Figure 7A**). These consist of intraformational normal faults that affect the Jurassic depositsof the El

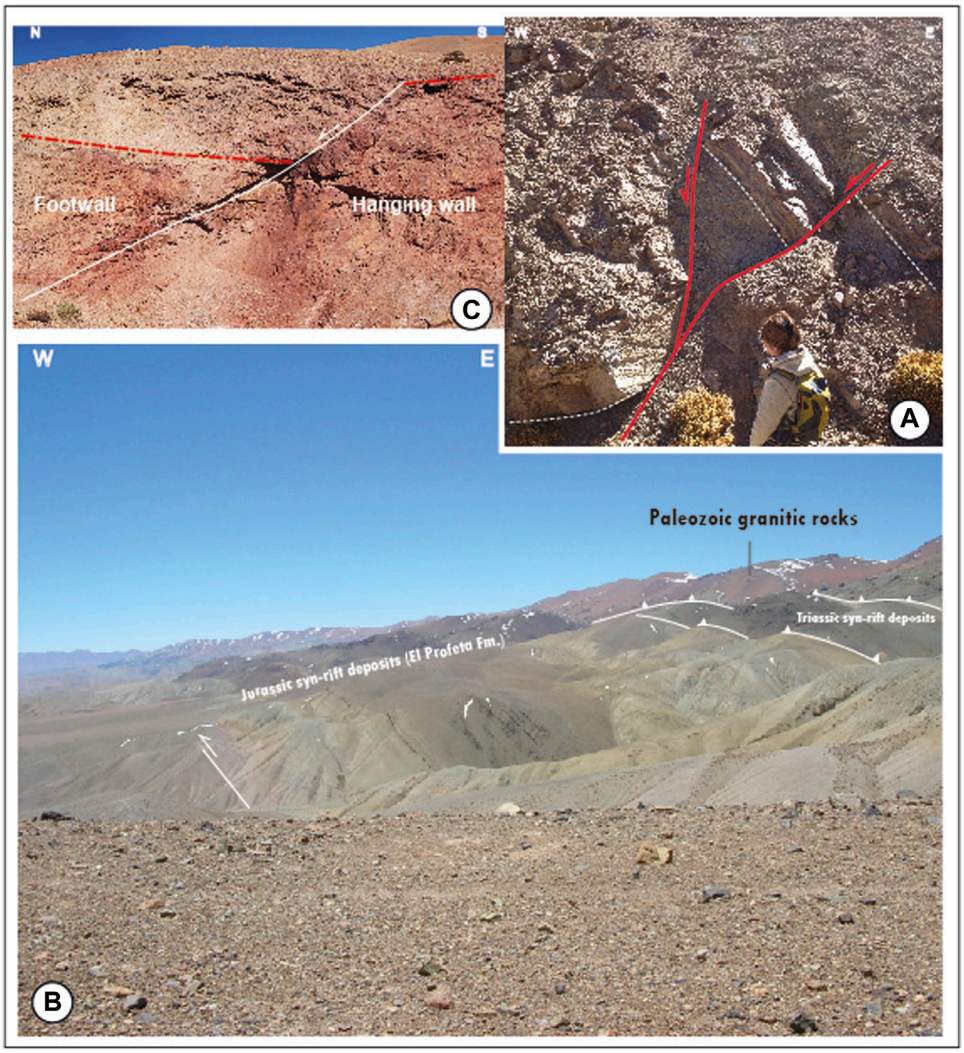

FIGURE 7 | (A) Aspectsof the mesoscopic normal faults found in the Jurassic syn-rift El Profeta Formation exposed along the Domeyko Cordillera, **(B)** hybrid (thick and thinskinned) fold-and-thrust belt affecting the Triassic and Jurassic syn-rift deposits exposed in the western Sierra de Varas sector of the Domeyko Cordillera (see **Figures 2**, **6A** for location), and **(C)** mesoscopic normal faults affecting the internal structure of the Permian La Tabla Formation in the Sierra de Almeida sector (see **Figure 3** for location).

ProfetaFormation. In neighboring sectors of the Sierra de Varas, these exhibit the greatest thickness at the hanging-wall blocks and form stratigraphic wedges that thicken along the fault planes related to syn-rift sequences (Espinoza et al., 2018). These syn-rift successions are incorporated into a narrow west-verging thick-skinned fold-and-thrust belt (Amilibia et al., 2008; Espinoza et al., 2018, **Figures 6**, **7B**). Similar stratal geometries are observed on the footwall of the Imilac fault in the eastern Domeyko Cordillera (**Figure 3**). Here, Upper Triassic sedimentary syn-rift successions of the Pular Formation lie on the footwall block of the fault, thus indicating that, possibly, an ancient Mesozoic rift-related depocenter is hidden under this sector of the Salar de Punta Negra Basin. Other mesoscopic evidence related to Late Permian crustal extension is recognized in the Sierra de Almeida, where some poorly preserved normal faults directly affect the Upper Permian volcanic deposits of the La Tabla Formation (**Figure 7C**). Along these faults, the strata of the La Tabla Formation exhibit an apparent greater thickness on the hanging wall than that in the footwall fault blocks, suggesting that normal faulting occurred during its accumulation.

Half-graben structures and syn-rift stratigraphic wedges are well identified in the 2D seismic profiles (**Figures 8**, **9**) located along the northern and central part of the basin, which correspond to a series of ancient and partially reactivated west- and east-dipping normal faults. The faults usually exhibit planar and semi-listric shapes with moderate dip angles in their upper sections (approximately 40°–60°) and penetrate down into the Paleozoic crystalline basement rocks. The fault planes are highlighted as thin and semicontinuous inclined reflectors that cut and separate seismic reflectors with

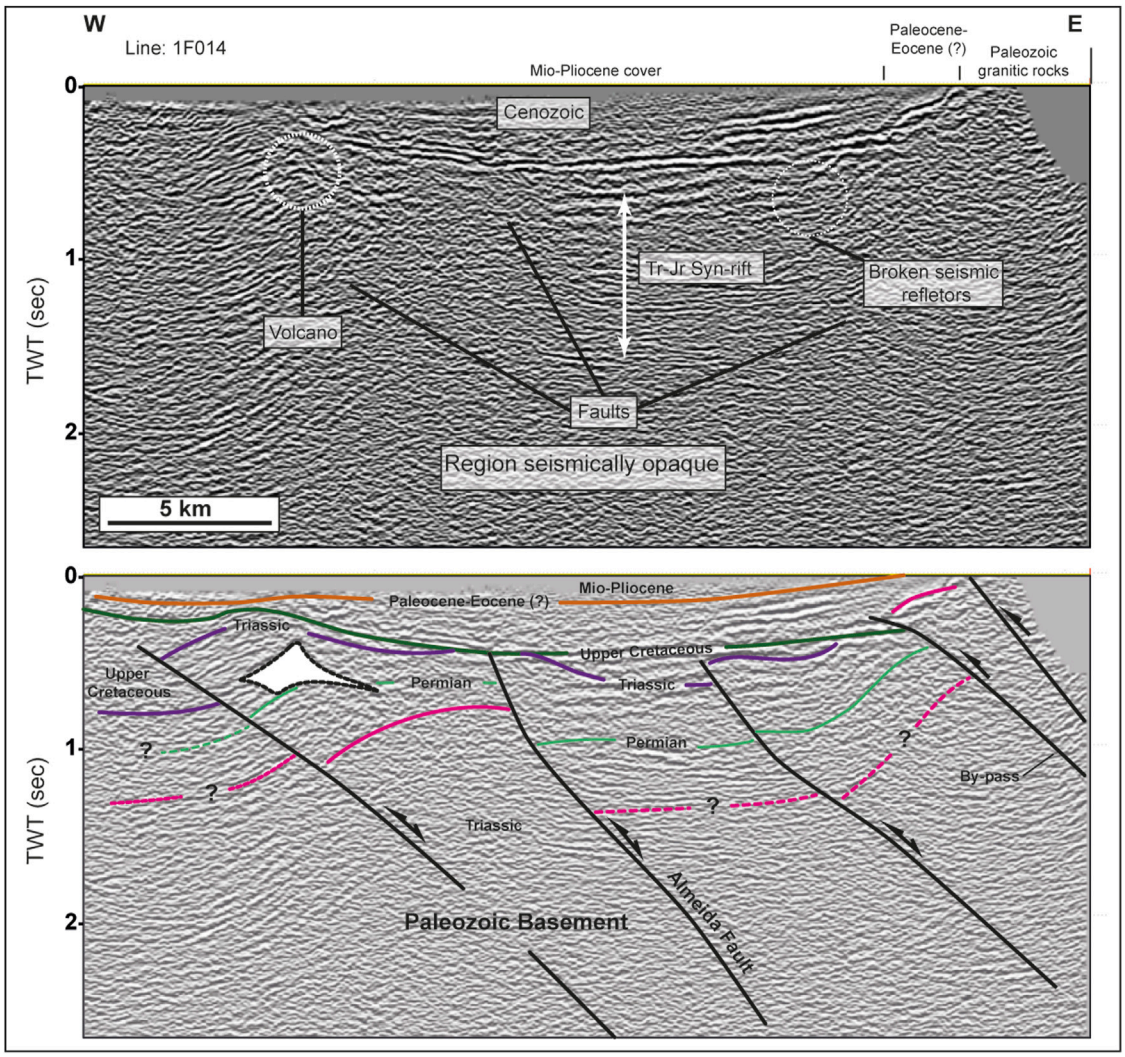

FIGURE 8 | (A) Uninterpreted central and eastern section of2D seismic profile 1F014 and **(B)** structural interpretation of 2D seismic profile 1F014 showing the presence of west-verging inversion anticlines and basement reverse faults under the central and eastern sections of the basin. Note the distribution of the Upper Cretaceous and Cenozoic synorogenic deposits over and along the structures.

different inclinations (**Figures 8**, **9**) and with different seismic reflection patterns (e.g., chaotic seismic reflectors versus parallel seismic reflectors). The hanging-wall fault blocks consist of tilted blocks overlain by parallel seismic reflectors and asymmetrical stratigraphic wedges composed of divergent and intercalated low and high amplitude seismic reflectors (**Figures 8**, **9**) related to Upper Permian–Jurassic deposits. The wedges get thicker near the fault planes and thinner over the shoulders of the half grabens, thus displaying a classical syn-rift stratigraphic architecture (**Figure 9**).

The shallow seismic reflectors of the youngest syn-rift sequences correlate with the Jurassic sedimentary successions of the El Profeta Formation (**Figures 8**, **9**), whereasthe deeper ones correlate with the Permian stratified rocks of the La Tabla Formation (**Figure 9**). Some deepest parallel seismic reflectors could be correlated with the Devonian Zorritas Formation; however, there is no subsurface information (e.g., well data) that supports this interpretation. Based on the seismic patterns and the stratigraphic and structural relationships described here, we interpret that the region was initially affected by a regional-scale crustal extension from at least the Late Paleozoic (Permian) to the Jurassic times, thus creating an asymmetrical extensional system.

4.2 Evidence of Basin Inversion

The main evidence of inverted structures is recognized from the 2D seismic profiles presented in this study. These data show that the syn-rift deposits in the hanging-wall fault blocks form either west- or east-verging asymmetrical anticlines, depending on the initial normal fault dip direction (**Figures 8**, **9**). Along the anticlines, the tops of the syn-rift successions are elevated over their original positions (or regional data). Geometrically, these

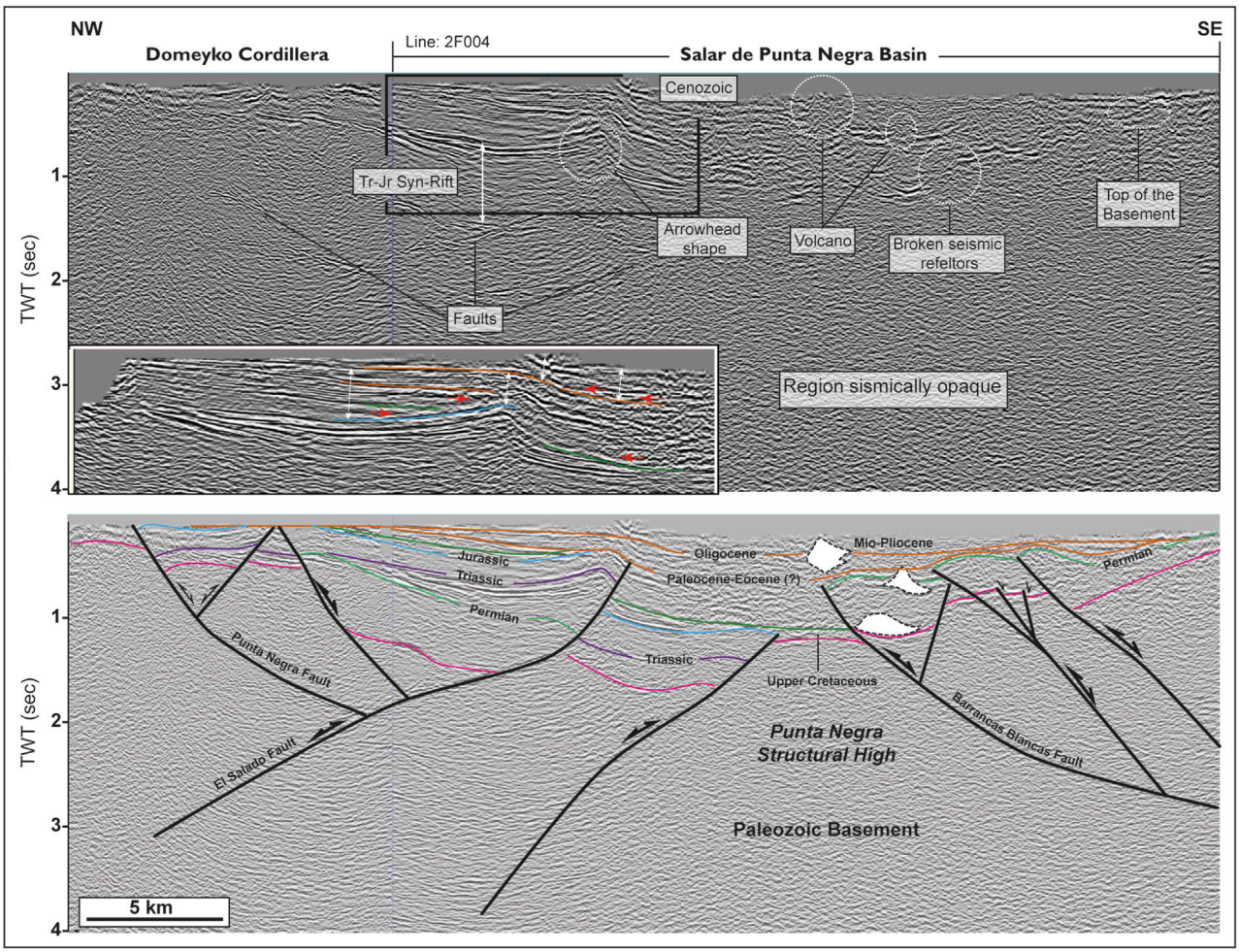

FIGURE 9 | (A) Uninterpreted2D seismic profile 2F004 and detail of the shallow seismic reflectors over the contractional structures and related to synorogenic strata. Note the thinning of these over the anticline, which is typical of contractional growth strata. The red arrows indicate on-lap terminations **(B)** structural interpretation of seismic profile 2F004 evidencing the presence of doublyverging (E–W) inverted structures under the central part of the Salar de Punta Negra Basin. Note the geometry and distribution of the syn-rift on the hanging-wall blocks of the partially inverted half-graben structures and the synorogenic deposits over the inversion anticlines.

are composed of short and steeply dipping forelimbs and large and semi-horizontal back limbs, thus creating an asymmetrical anticline, such as those reported by the inversion anticlines created from the reverse-reactivation of normal faults (McClay, 2002; **Figures 8**, **9**). A series of small cone-shape bodies also are recognized at the core of the anticlines (**Figures 8**, **9**). Internally these exhibit chaotic seismic reflectors cutting the regional stratification with a flat base, a typical geometry of volcanic bodies. These could correspond to ancient and fossilized volcanic cones, considering that many of they lie well exposed to the southern part of the basin. The forelimbs are truncated against the fault planes, preferably along their upper segment. This is well recognized in the Almeida, Barrancas Blancas El Salado, and Punta Negra faults (**Figures 8**, **9**). The 2D seismic profile 1F014 shows the existence of three west-verging anticlines under the northern section of the basin. Both are established on the hanging wall of previous Permian and Triassic extensional faults (e.g., the Almeida fault, **Figure 8**). The faults display normal slip in their lower segments and reverse slip along the uppermost segments, thus indicating a partial reverse reactivation following the classification provided by Bally (1984).

In the central section of the basin, the 2D seismic profile 2F004 also shows the existence of several west-and east-verging inverted structures separated by the Punta Negra structural high (**Figure 9**). In the western section, the hanging wall of the previous synthetic (e.g., El Salado fault) and antithetic normal faults (e.g., the Punta Negra fault) correspond to asymmetrical anticlines affecting the Permian–Jurassic syn-rift, which are expelled from basement half-graben structures (**Figure 9**). In the eastern section of the seismic profile, a series of east-verging anticlines are recognized (**Figure 9**). These mainly involve the Upper Permian deposits of the La Tabla Formation, which is tectonically elevated over the top of the Punta Negra structural high (**Figure 9**). The faults consist of semi-listric (e.g., the Barrancas Blancasfault) and planar faults. In this region, the Barrancas Blancas fault exhibit full reverse reactivation,

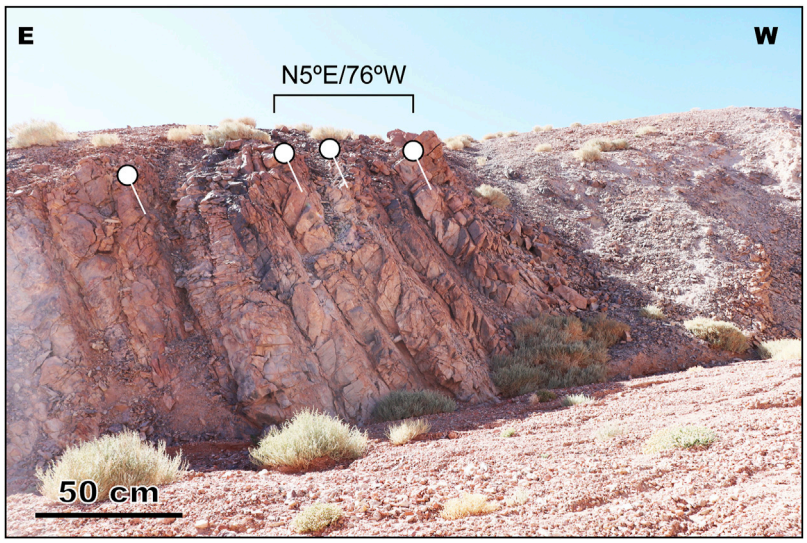

FIGURE 10 | Local view of the west-dipping decameter-scale beds of intercalated quartzites, sandstones, and shales of the Zorritas Formation exposed in the mountain front of the Sierra de Almeida (see **Figure 3** for location of the photographs).

considering that the top of basement pre-rift at the hanging wall block is elevated over its initial position on the footwall block, whereas the others were partially inverted, because maintain a reverse slip on the upper segment of the faults and a normal slip on the lower segments; furthermore, some minor faults were not reactivated (**Figure 9**).

4.3 Other Contractional Structures

In addition to the normal and inverted structures, several basement-involved east- and west-verging faults are well exposed along the western and northeastern margins of the basin (**Figure 3**). They consist of reverse faults (e.g., the Imilac, Pan de Azucar, Cachiyuyo, and Agua Amarga faults) that affect both the footwall and hanging wall of the inverted normal faults present in the subsurface and previously described. The hanging wall of the west-dipping Imilacfault is a kilometer-scale block superimposed on the Upper Triassic syn-rift deposits of the Pular Formation (**Figure 3**). Previous structural interpretations of2D seismic profiles through the fault indicated the presence of a blind and partially inverted Triassic half-graben structure in the footwall block (Martínez et al., 2020). Other structures, such as the west-verging Agua Amargafault (**Figure 3**), mark the eastern termination of the innermost part of the current volcanic arc. Its hanging-wall block is a broad west-verging basement-cored anticline along which the Paleozoic units of the Imilac Complex have been elevated over 2.5 km. The sedimentary beds of the Paleozoic Zorritas Formation near the fault-plane contact are highly sheared and steeply dipping (**Figure 10**), a sign of significant shortening experienced by these structures. Usually, the basement reverse faults cut the Pliocene–Pleistocene deposits that form the cover of the basin, thus revealing a Late Cenozoic activity. The2D seismic profile 1F014 (**Figure 8**) shows an important west-verging basement-involved reverse fault under the eastern section of the basin. This is affecting the hanging wall of a partially inverted normal fault with a style similar to the reported by by-pass faults (Bonini et al., 2012; **Figure 8**).

4.4 Evidence of Late Cretaceous–Cenozoic Synorogenic Deposition

In the northern Salar de Punta Negra Basin, specifically at the footwall of the Pan de Azucarfault (**Figure 3**), contractional growth strata lie preserved along synclines involving the Paleocene–Eocene Naranja Formation (**Figure 5A**). Recent works (Solari et al., 2017; Martínez et al., 2019) have reported the U–Pb ages for detrital and volcanic zircons of this unit that range approximately between 60 and 55 Ma. Although the field evidence might be insufficient, the 2D seismic data (**Figure 9**) show shallow and intermediate seismic reflection patterns forming fan shapes over contractional structures, such as inversion anticlines and/or the forelimbs of basement reverse faults, which are the most robust evidence of synorogenic accumulation. The seismic reflectors exhibit an onlapping with growth strata over the crest and forelimbs of the anticlines (**Figures 8**, **9**) and also over the flanks of the syncline folds. They form asymmetrical stratigraphic wedges that are thinner over the anticlines and thicker along the flanks, thus indicating that they were accumulated contemporaneously with contraction. Based on our field observations and the correlations with synorogenic successions exposed in neighboring basins (e.g., Salar de Atacama and Salar de Pedernales), we correlated the basal seismic reflectors of the synorogenic stratigraphic wedges with the Upper Cretaceous synorogenic deposits (e.g., Pajonales Formation; **Figure 3**), whereas those of the intermediate and shallow seismic reflectors are mostly related to Paleocene–Oligocene–Miocene synorogenic deposits.

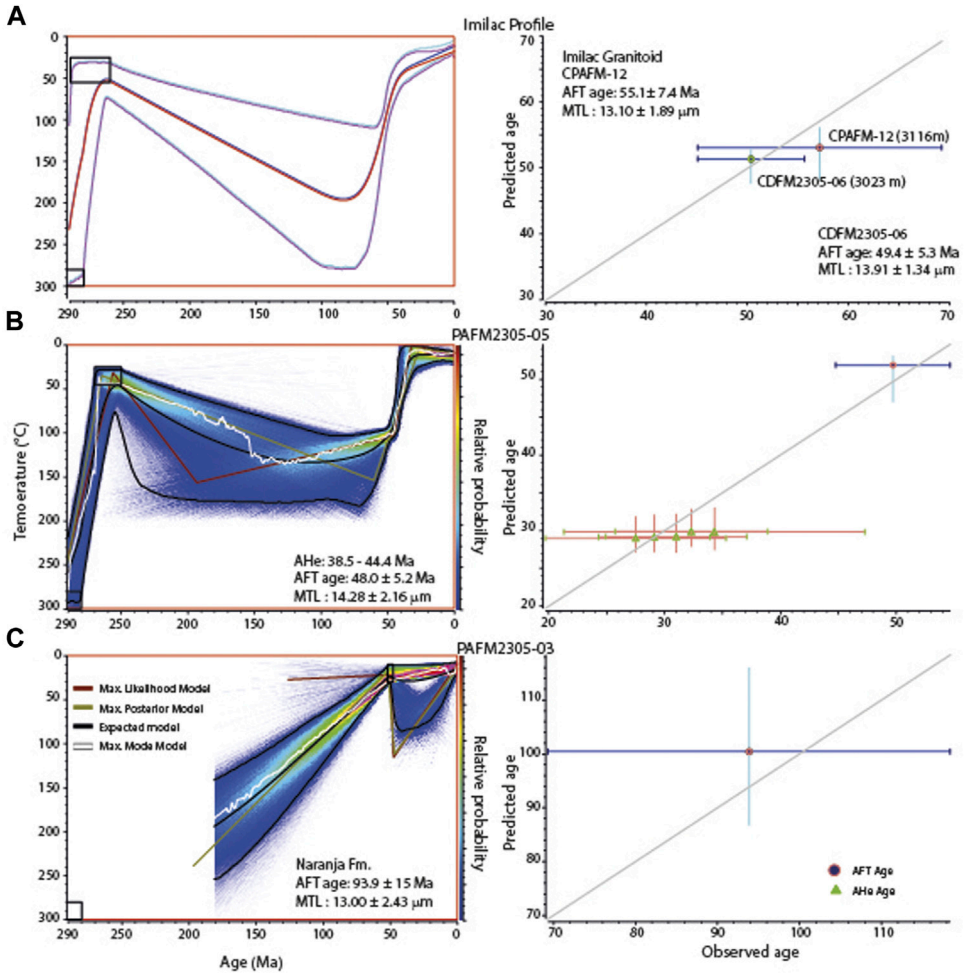

FIGURE 11 | QTQt models obtained for the granitic and sedimentary rock samples analyzed in this study (note that modeling lengths when only approximately 10 lengths were measured will not provide a good result): **(A)** model for granitic rocks exposed in the eastern Domeyko Cordillera on the hanging wall of the Imilacfault, **(B)** model for granitic rocks exposed on the hanging wall of the Pan de Azucarfault, and **(C)** model for a sedimentary rock sample of the Naranja Formation on the footwall of the Pan de Azucarfault.

4.5 Thermal History of Paleozoic Rocks

The three Permian granitic rocks that we analyzed (PAFM2305-03, CDFM2305-06 PAFM2305-05; and CPAFM12; **Table 1**) were collected from the hanging-wall blocks of the Imilac and Pan de Azucarfaults described previously (see **Section 4.3**; **Figure 3**). The samples consist of granodiorites and monzogranites, with reported U–Pb crystallization ages between 281 and 298 Ma (Solari et al., 2017). The samples were collected from both the top and bottom of the ranges, with elevations between 3,000 and 3,500 m. Samples CDFM2305-06 and CPAFM12 (**Figure 3**), located ~11 km apart in the hanging wall of the Imilac fault at 3023 and 3,116 m of elevation, respectively, yielded concordant AFT central ages of 49.4 ± 5.3 and 55.1 ± 7.4 Ma, with relatively long mean track lengths of 13.91 ± 1.34 µm (CDFM2305-06) and 13.10 ± 1.89 µm (CPAFM12) (**Table 1**; **Supplementary Data S1**). The AFT data define an age elevation trend, with older ages at higher elevations (**Figure 11A**). Thermal modeling shows that Permian granitic rocks were cooled rapidly and exhumed through the partial annealing zone between the Paleocene (~60 Ma) and Eocene (~40 Ma), as illustrated in **Figure 11**. Our thermochronological results are in agreement with the post–Late-Cretaceous uplift constrained mainly by the Upper Cretaceous synorogenic deposits reported in the footwall block of this structure in neighboring regions (e.g., Domeyko Cordillera, Salar de Atacama Basin; Arriagada et al., 2006; Bascuñán et al., 2016, Bascuñán et al., 2019; Henriquez et al., 2018; Martínez et al., 2018).

Sample PAFM2305-05 from the hanging-wall block of the Pan de Azucarfault (**Figure 3**; **Table 1**) yields a concordantAFT age of 48.0 ± 5.2 Ma, with a mean track length of 14.28 ± 2.16 µm. In addition, five aliquots analyzed for AHe yielded reproducible ages ranging between 44.4. ± 0.6 and 38.5 ± 0.5 Ma (**Table 2**). Despite a large variation in the effective uranium contents, from 83 to 155 ppm, reproducible ages indicated that limited radiation damage accumulated over the cooling history. Altogether, the thermochronological data suggest rapid cooling sometime

TABLE 2 | Apatite (U/Th)/He data reported in this study.

Sample	Ft-corrected age (Ma)	2σ (Ma)	U (ppm)	Th (ppm)	^{147}Sm (ppm)	[U]e (ppm)	Th/238U	He (nmol/g)	Mass (ug)	Ft	ESR (mm)
PAFM2305-05_a1	38.5	0.5	61.4	93.0	31.1	83.2	1.6	13.2	2.84	0.76	56.8
PAFM2305-05_a2	44.4	0.6	30.0	38.4	16.5	39.0	1.3	7.3	3.50	0.77	62.7
PAFM2305-05_a3	42.0	0.4	68.6	66.2	22.2	84.1	1.0	14.8	3.31	0.77	60.4
PAFM2305-05_a4	42.1	0.5	60.9	69.0	23.6	77.1	1.2	13.0	3.27	0.74	57.7
PAFM2305-05_a5	38.5	0.6	129.9	109.0	59.6	155.5	0.9	23.2	1.82	0.71	54.8

between 60 and 35 Ma and limited cooling thereafter, which we interpret as the result of Eocene thrusting along the Pan de Azucar fault. The thermal models (**Figure 11A**) show time–temperature paths similar to the multisample model of CDFM2305-06 and CPAFM12, which suggests coeval reverse faulting along the Imilac and Pan de Azucar faults. Furthermore, this Eocene exhumation is also recorded by the Eocene synorogenic deposits of the Naranja Formation exposed on its footwall block (**Figure 3**; Martínez et al., 2020). There, sample PAFM2305-03, collected in the lower Eocene strata of the Naranja Formation, yields a discordant AFT central age of 93.9 ± 15.0 Ma with a shorter mean track length of 13.00 ± 2.43 μm in annealing-resistant apatites with a mean Dpar value of 2.80 μm.An AFT age older than the stratigraphic age documents that this age is, at most, partially reset, due to insufficient burial in the footwall of the Pan de Azucarfault. Such a scenario is captured in the thermal model presented in **Figure 11C**.

5 DISCUSSION

5.1 Permian to Mesozoic Crustal Extension

Our mesoscale field observations together with the analysis of 2D seismic profiles showed evidence of extensional structures, which were active during both periods. The pre-shortening restorations (**Figures 12A–C**) of a regional cross section extended from the eastern Domeyko Cordillera to the innermost part of the present-day volcanic arc show a pre-Andean (or precontraction) tectonic setting dominated by half-graben structures, along which the Permian La Tabla, Triassic Pular, and Jurassic El Profeta Formations were accumulated. Previous studies (Kay et al., 1989; Mpodozis and Kay, 1990, Breitkreuz, 1990; Charrier et al., 2007; Maksaev et al., 2014; Morandé et al., 2015, among others), mostly supported by U–Pb dating and geochemical analyses of Upper Paleozoic intrusive and volcanic rocks, have suggested that an extensional arc magmatic setting was active along the present-day Domeyko Cordillera during the Late Paleozoic, however; major structural evidence and details on the 2D geometry and kinematic evolution of the Permian extensional faults hidden in the pre-Andean basins of northern Chile have not been reported.

The causes of a Late Permian tectonic extension in northern Chile are a matter of debate. Some researchers considered a crustal extension related to geodynamic rollback subduction, which allowed the establishment of back-arc extensional basins (Mpodozis and Kay, 1990; Breitkreuz, 1991; Charrier et al., 2007; Maksaev et al., 2014). Others (Bahlburg and Breitkreuz, 1991; Semperé et al., 1997; Amilibia et al., 2008) interpreted a Late Paleozoic crustal extension as induced by enhanced mantle convection, similar to the pure shear mode of McKenzie (1978) and (Wernicke, 1981). Crustal extension developed large and narrow intracontinental rift systems extending from Central Perú (Arequipa Basin) to northern Chile (Tarapacá Basin), along which thick silica-rich volcanic products and continental sedimentary successions accumulated (Semperé et al., 2002). Regardless of both initial interpretations, we confirmed the existence of Upper Permian east- and west-dipping normal faults bounding halfgrabens under the pre-Andean Depression. Our confirmation supports the notion that Permian crustal extension dominated a significant part of the Late Paleozoic tectonic evolution of the Central Andes (Mégard, 1978; Tankard et al., 1995; Semperé et al., 2002; Ramos, 2009). Our tectonic reconstructions (**Figure 12A**) indicate that two large half-graben structures developed along the western and eastern sections of the study area.

The seismic tectonic sequences associated with the Upper Triassic (Pular Formation), and Jurassic (El Profeta Formation) deposits display similar stratigraphic and structural relationships to those shown by the Permian La Tabla Formation. Such relationships have also been recognized in several regions of northern Chile (Amilibia et al., 2008; Mpodozis and andRamos, 2008; Martínez et al., 2016; Fuentes et al., 2018; López et al., 2019; Martínez et al., 2019), thus indicating that initial Late Paleozoic crustal extension propagated through the Triassic and Jurassic. Following the kinematic evolution of rift systems proposed from field and experimental studies (McClay et al., 2002; Ziegler and Cloetingh, 2004; Corti, 2012; Corti et al., 2018, among others), these could have taken advantage of pre-existing weaknesses during the initial stages of crustal extension, such as ancient faults, fold axes, suture zones, and regional-scale foliations, among others, which are difficult to identify in the study area.

Accordingly, we propose that the Mesozoic syn-rift sequences were controlled tectonically by the negative reactivation of the

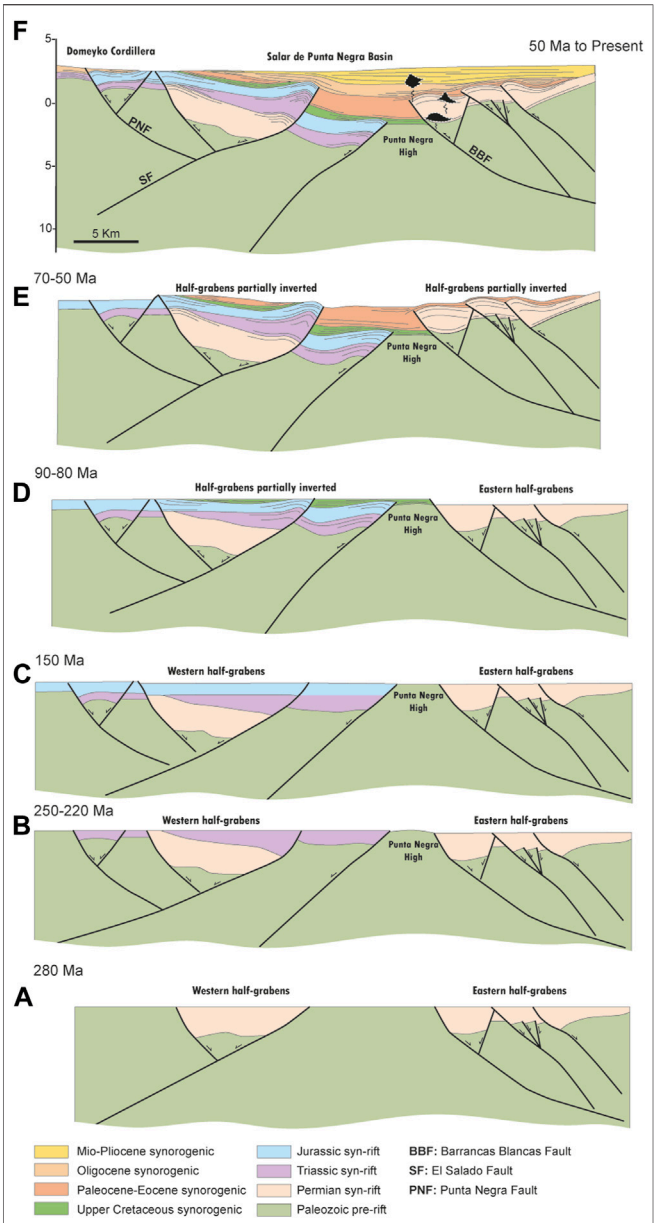

FIGURE 12 | Sequential restoration of a regional-scale crosssection constructed from integration of field data (dips and stratigraphic thicknesses) and structural information from 2D seismic profile 2F004: **(A)** Late Permian tectonic extension and creation of half-graben structures, **(B)** Triassic tectonic extension, **(C)** Jurassic tectonic extension, **(D)** Late Cretaceous selective reversereactivation of previous normal faults and accumulation of Upper Cretaceous synorogenic deposits, **(E)** Paleocene–Eocene contraction allowing a second episode of reversereactivation of the previous normal faults, and **(F)** Oligocene to recent contraction and final configuration of the present-day structure of the Salar de Punta Negra Basin. The restoration was constructed using the StructureSolver software (www.structuresolver.com).

previous Permian normal faults, such as is evidenced from the tectonic restorations (**Figures 12B,C**), and by the creation of new normal faults on the eastern Domeyko Cordillera and the central section of the Salar de Punta Negra Basin. All the interpretations discussed above significantly improve the recent interpretations by Espinoza et al. (2018), who proposed that the crustal extension in the region started ca. 240 Ma ago.

Considering various previous and recent interpretations in neighboring pre-Andean basins (e.g., Salar de Atacama, Salar de Pedernales, and Calama Basins; Muñoz et al., 2002; Mpodozis et al., 2005; Amilibia et al., 2008; Martínez et al., 2018, Martínez et al., 2020, Espinoza et al., 2018; López et al., 2019), where similar extensional structure-related rifts have been recognized, our interpretation is that the pre-Andean Depression was a region of significant pre-orogenic intracontinental weakness. This possibly acted as an elongated crustal depression bounded on one or both sides by basement-involved normal faults, and its axis possibly coincided with the present-day location of the salt flats. The presence of Lower Jurassic deposits along inverted half grabens in neighboring regions, such as the Domeyko Cordillera, Salar de Atacama Basin, Salar de Pedernales Basin, and the Frontal Cordillera of northern Chile, suggests that the crustal extension continued up to Early Jurassic times.

5.2 Late Cretaceous–Cenozoic Contraction

The basal seismic reflectors related to Upper Cretaceous tectonic sequences onlapping on the top of the inversion anticlines indicates that the crustal contraction began in the Late Cretaceous from the reverse reactivation of the previous Permian to Mesozoic half-graben structures (**Figure 12D**). This contraction was marked by the creation of doubly verging inversion anticlines that developed the early topographic relief in the region. Previous regional studies in northern Chile (e.g., studies of the Domeyko Cordillera, Coastal Cordillera, and pre-Andean Depression; Arriagada et al., 2006; Amilibia et al., 2008; Bascuñán et al., 2016; López et al., 2017, Bascuñán et al., 2019; Fuentes et al., 2018; Henriquez et al., 2018) have also reported a Late Cretaceous age for the onset of the Andean Orogenesis, as it is mainly related to the tectonic inversion of extensional structures of the Tarapacá Basin. Based on the abovementioned studies, the tectonic inversion is interpreted as a generalized mechanism active during the initial growth of the Central Andes of northern Chile. However, in the Salar de Punta Negra Basin, the basin inversion continued during the Cenozoic, as recorded by the Cenozoic synorogenic deposits covering the inversion anticlines (**Figures 12D–F**).

The tectonic restorations shown in **Figure 12** indicate that much ofthe basin inversion was acquired during the Paleocene–Eocene. During this period, some faults located in the easternmost region of the basin were fully inverted and the faults located in the central section (e.g., El Salado fault, **Figure 13**) were reactivated, thus creating a contractional basin between them (**Figures 12E**,F, **13**). The last suggests that the Cenozoic subsidence of the basin and the neighboring regions into the pre-Andean Depression was controlled by the progressive growth of the large inverted structures, such as it is presented in a tridimensional model (**Figure 13**; **Supplementary Data S2**), and not by tectonic extension or strike–slip faulting, as was initially proposed by Pananont

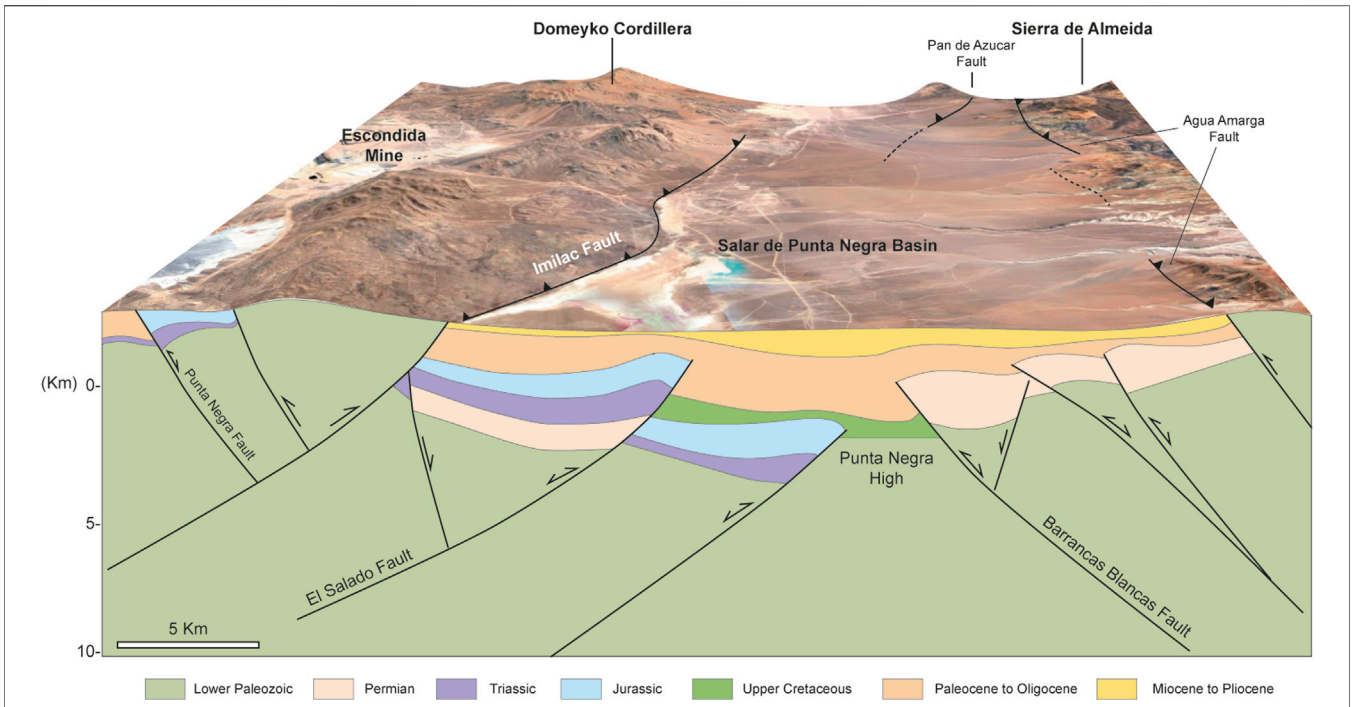

FIGURE 13 | Tridimensional model of the central section of the Salar de Punta Negra basin, showing the correlation and distribution of the main structures recognized on the field, and the seismic profiles presented in this work. The model was constructed using Andino 3D software (www.andino3.com.ar).

et al. (2004) and Jordan et al. (2002), who interpreted the Cenozoic deformation in the region as the result of short-lived contractional and/or neutral and extensional tectonic conditions associated with periods of high and low convergence rates. The Late Cretaceous crustal shortening of the western Central Andes and the onset of the basin inversion are related to the absolute trenchward motion of the overriding plate (South American) from the opening of the Atlantic Ocean (Cobboldet al., 1995; Jaillard and Soler, 1996; Semperé et al., 1997), which led to changes in the regional field stress from extensional to contractional in the continental margin. Recently, similar tectonic conditions have been interpreted in several retroarc regions of the southern Central Andes (Gianni et al., 2018; Gianni and NavarreteandSpagnotto, 2019).

The final episodes of basin inversion were accompanied by significant basement deformation dominated by doubly verging reverse faulting, from which the current east and west tectonic bounds of the basin developed (**Figure 13**). The timing of this deformationin the region has been mainly constrained by the analysis of AFT data and also by the youngest Cenozoic synorogenic deposits exposed over the footwall blocks of the faults, indicating that the deformation started at least from the Eocene. The timing of reverse faulting was also detected from our AFT data, indicating that a significant cooling episode caused by exhumation of the kilometer-scale basement blocks occurred at this time. This episode is correlated with the so-called Incaic tectonic phase proposed by Steinman (1929), which is responsible for major basement deformation and uplift in the western Central Andes.

Recent U–Pbdating analyses of granitic clasts contained within Eocene–Oligocene and Miocene synorogenic successions exposed in the western Salar de Atacama Basin (Henriquez et al., 2018) have reported Permian ages, confirming that Permian granitic rocks were uplifted tectonically and eroded during the Cenozoic. The basement reverse faulting was favored possibly by the Late Cretaceous to the Miocene–Pliocene eastward migration of the magmatic arc (Bascuñan et al., 2016). This migration led to a rise in the geothermal gradient in the upper crust and, therefore, conditions most favorable to the development of basement-involved tectonics. Several large basement reverse faults cut Pliocene and Pleistocene volcanic and sedimentary rocks, indicating that the inner forearc and the pre-Andean Depression are currently under tectonic contraction.

6 CONCLUSION

The Late Paleozoic–Cenozoic tectonic evolution of the Salar de Punta Negra Basin and the inner Andean forearc in general is characterized by several episodes of crustal extension and contraction, thus reflecting its complex history during the evolution of the Central Andes in northern Chile. The field and 2D seismic data show significant evidence of extensional tectonic activity occurring between the Late Permian and the Triassic and possibly continuing through the Early Jurassic, related to the initial breakup and subsequent stretching of western Gondwana. The evidence comprises half-graben

basement structures bounded by listric west- and east-dipping normal faults. Along these structures, thick volcanic and sedimentary marine successions accumulated contemporaneously, thereby forming typical stratigraphic wedge-related syn-rift deposits. From the Late Cretaceous to the Paleocene, the previous extensional structures were reactivated partially because of basin inversion, which transformed the tectonic setting from extensional to contractional. During this process, the Permian–Mesozoic syn-rift deposits were expelled from the halfgrabens, creating doubly verging inversion anticlines that developed the initial topographic relief in the region. The initial interplay between contraction, tectonic uplift, and erosion is marked by the accumulation of basal, thick Upper Cretaceous–Paleocene synorogenic volcanic and sedimentary deposits over and along the inverted structures. The basin inversion was accompanied by basement reverse faulting, which started during the Eocene (Incaic tectonic phase) and continued up to the Pleistocene. Several basement reverse faults acted as break thrusts and/or truncated a number of the previously inverted normal faults, thereby uplifting the hanging-wall and footwall blocks of the ancient extensional systems. Further, this last process facilitated the cooling by exhumation of the pre-rift basement rocks of the basin, which acted as important sources of sediments that filled the basin during the Cenozoic.

Our interpretation is that the current structural and topographic configuration of the pre-Andean Depression was developing at least from the Paleocene. These reverse faults are the most favorable structures to produce the crustal thickening under the Andean forearc.

DATA AVAILABILITY STATEMENT

The original contributions presented in the study are included in the article/**Supplementary Material**, further inquiries can be directed to the corresponding author.

AUTHOR CONTRIBUTIONS

FM: writing, editing, and geological interpretations MP: writing and thermochronological modeling RG: editing and structural interpretations CL: field geological supporting ES: analysis of AFT data JG: analysis of AFT data The rest of the authors collaborated during the collection of field geological data.

FUNDING

This study was supported by the AgenciaNacional de Investigación y Desarrollo (ANID) Research Project PCI-2019/133349- 8 "Tectono-stratigraphic evolution of intermontane basins related to forearc tectonic settings using the Chilean Pre-Andean Depression of the Central Andes as a case study." The structural modeling software packages StructureSolver and Andino 3D were facilitated by Nunns and Rogan Company, and LA. TE Andes, respectively.

ACKNOWLEDGMENTS

We thank ENAPSipetrolfor providing the 2D seismic data used in this study. Finally, we thank the constructive reviews of two reviewers and Dr. Nicholas Pérez, which help to improve the previous version of this contribution.

SUPPLEMENTARY MATERIAL

The Supplementary Material for this article can be found online at: https://www.frontiersin.org/articles/10.3389/feart.2021.790526/full#supplementary-material

Supplementary Data S1 | Radial plots of fission track ages for all samples analyzed in this study.

Supplementary Data S2 | Tridimensional distribution of the main structures recognized in the Salar de Punta Negra Basin from 2-D seismic profiles.

REFERENCES

Amilibia, A., Sàbat, F., McClay, K. R., Muñoz, J. A., Roca, E., and Chong, G. (2008). The role of inherited tectono-sedimentary architecture in the development of the central Andean mountain belt: insights from the Cordillera de Domeyko. *J. Struct. Geology.* 30 (12), 1520–1539. doi:10.1016/j.jsg.2008.08.005

Arriagada, C., Cobbold, P. R., and Roperch, P. (2006). Salar de Atacama basin: A record of compressional tectonics in the central Andes since the mid-Cretaceous. *Tectonics* 25 (1), a–n. doi:10.1029/2004TC001770

Bahlburg, H., and Breitkreuz, C. (1991). Paleozoic Evolution of Active Margin Basins in the Southern Central Andes (Northwestern Argentina and Northern Chile). *J. South Am. Earth Sci.* 4 (3), 171–188. doi:10.1016/0895-9811(91)90029-k

Bally, A. W. (1984). Tectogenese et sismique reflexion. *Bull. Soc.Géol. France* S7-XXVI (2), 279–285. doi:10.2113/gssgfbull.s7-xxvi.2.279

Bascuñán, S., Arriagada, C., Le Roux, J., and Deckart, K. (2016). Unraveling the Peruvian Phase of the Central Andes: stratigraphy, sedimentology and geochronology of the Salar de Atacama Basin (22°30-23°S), northern Chile. *Basin Res.* 28 (3), 365–392. doi:10.1111/bre.12114

Bascuñán, S., Maksymowicz, A., Martínez, F., Becerra, J., Arriagada, C., and Deckart, K. (2019). Geometry and late Mesozoic-Cenozoic evolution of the Salar de Atacama Basin (22°30′-24°30′S) in the northern Central Andes: New constraints from geophysical, geochronological and field data. *Tectonophysics* 759, 58–78. doi:10.1016/j.tecto.2019.04.008

Breitkreuz, C. (1990). "Late Carboniferous to Triassic Magmatism in the Central and Southern Andes: the Change from an Accretionary to an Erosive Plate Margin Mirrors the Pangea History," in *Symp Int Géodyn Andin* (Paris: ORSTOM Coll Sèmin), 359–362.

Breitkreuz, C. (1991). Permo-Carboniferous Magmatism, basin Development, and Tectonics in the north Chilean Andes. *XII Int. Congress Carboniferous andPermian Geology. Stratigr. Abstr.*, 17–18.

Cecioni, A., and Frutos, J. (1975). Primera noticia sobre el hallazgo de Paleozoico inferior marino en la Sierra de Almeida, norte de Chile. *Congr. Argent. Paleontol. Bioestrat.* 1, 191–207. Actas1, Tucumán, 1974.

Charrier, R., Pinto, L., and Rodríguez, M. P. (2007). "Tectonostratigraphic Evolution of the Andean Orogen in Chile," in *"in the Geology of Chile*. Editors T. Moreno and W. Gibbons (London: The Geological Society), 21–114.

Chong, G. (1973). *Reconocimiento geológico del área Catalina-Sierra de Varas y estratigrafía del Jurásico del Profeta, provincial de Antofagasta. Memoria de*

prueba. (Santiago de Chile: Departamento de Geología, Universidad de Chile), 284.

Cobbold, P. R., Szatmari, P., Demercian, L. S., Coelho, D., and Rosello, E. A. (1995). "Seismic and Experimental Evidence for Thin-Skinned Horizontal Shortening by Convergent Radial Gliding on Evaporites, Deep-Water Santos Basin," in *Brazil" in Salt Tectonics: A Global Perspective*. Editor M.P.A. Jackson, et al. American Association of Petroleum Geologists Memoir, 65, 305–321.

Corti, G. (2012). Evolution and Characteristics of continental Rifting: Analog Modeling-Inspired View and Comparison with Examples from the East African Rift System. *Tectonophysics* 522-523, 1–33. doi:10.1016/j.tecto.2011.06.010

Corti, G., Molin, P., Sembroni, A., Bastow, I. D., and Keir, D. (2018). Control of Pre-rift Lithospheric Structure on the Architecture and Evolution of Continental Rifts: Insights from the Main Ethiopian Rift, East Africa. *Tectonics* 37 (2), 477–496. doi:10.1002/2017tc004799

Cristallini, E., Giambiagi, L., and Allmendinger, R. (2004). True Three-Dimensional Trishear: A Kinematic Model for Strike-Slip and Oblique-Slip Deformation. *GSA Bull.* 116 (7-8), 938–952. doi:10.1130/b25273.1

Dumitru, T. A. (1993). "A New Computer-Automated Microscope Stage System for Fission-Track Analysis," in *Nuclear Tracks and Radiation Measurements*. Editor S.A. Durraniet al. (Oxford: Pergamon Press), 21, 575–580. doi:10.1016/1359-0189(93)90198-i*Nucl. Tracks Radiat. Measurements*

Erslev, E. A. (1991). Trishear Fault-Propagation Folding. *Geol* 19, 617–620. doi:10.1130/0091-7613(1991)019<0617:tfpf>2.3.co;2

Espinoza, M., Montecino, D., Oliveros, V., Astudillo, N., Vásquez, P., Reyes, R., et al. (2018). The Synrift Phase of the Early Domeyko Basin (Triassic, Northern Chile): Sedimentary, Volcanic, and Tectonic Interplay in the Evolution of an Ancient Subduction-Related Rift basin. *Basin Res.* 31, 4–32. doi:10.1111/bre.12305

Farley, K. A. (2002). U-Th)/He Dating: Techniques, Calibrations, and Applications. *Rev. Mineralogy Geochem.* 47 (1), 819–844.

Farley, K. A., Wolf, R. A., and Silver, L. T. (1996). The Effects of Long Alpha-Stopping Distances on (U-Th)/He Ages. *Geochimica et Cosmochimica Acta* 60, 4223–4229. doi:10.1016/s0016-7037(96)00193-7

Flint, S., Turner, P., Jolley, E. J., and Hartley, A. J. (1993). Extensional tectonics in convergent margin basins: An example from the Salar de Atacama, Chilean Andes. *GSA Bulletin105* 105 (5), 603–617. doi:10.1130/0016-7606(1993)105<0603:eticmb>2.3.co;2

Flowers, R. M., Ketcham, R. A., Shuster, D. L., and Farley, K. A. (2009). Apatite (U-Th)/He Thermochronometry Using a Radiation Damage Accumulation and Annealing Model. *Geochimica et Cosmochimica Acta* 73 (8), 2347–2365. doi:10.1016/j.gca.2009.01.015

Fuentes, G., Martínez, F., Bascuñan, S., Arriagada, C., and Muñoz, R. (2018). Tectonic Architecture of the Tarapacá Basin in the Northern Central Andes: New Constraints from Field and 2D Seismic Data. *Geosphere* 14 (6), 2430–2446. doi:10.1130/ges01697.1

Galbraith, R. F. (2005). *Statistics for Fission Track Analysis*. 1st ed. Chapman and HallBoca Raton CRC Press. doi:10.1201/9781420034929

Gallagher, K. (2012). "Uplift, Denudation, and Their Causes and Constraints over Geological Timescales," in *Regional Geology and Tectonics: Principles of Geologic Analysis*. Editors D.G. Roberts and A.W. Bally (Elsevier), 608–644. doi:10.1016/B978-0-444-53042-4.00022-4

Gardeweg, M., Pino, H., Ramírez, C. F., and Davidson, J. (1994). Mapa Geológico del área de Imilac y Sierra Almeida, Región de Antofagasta. *Serv. Nac. Geol. Min. Doc. Trab.* 7 (1). 100.000.

Giambiagi, L. B., Tunik, M., Barredos, S., Bechis, F., Ghiglione, M., Álvarez, P., et al. (2009). Cinemática de apertura del sector norte de la cuenca neuquina. *Rev. La. Asoc. Geológica Argentina* 65, 278–292.

Gianni, G. M., NavarreteandSpagnotto, C. S., and Spagnotto, S. (2019). Surface and Mantle Records Reveal an Ancient Slab Tear beneath Gondwana. *Sci. Rep.* 9 (1), 19774–19810. doi:10.1038/s41598-019-56335-9

Gianni, G. M., Echaurren, A., Fennell, L., Navarrete, C., Quezada, P., Tobal, J., et al. (2018). "Cretaceous Orogeny and Marinetransgression in the Southern Central and Northern Patagonian Andes: Aftermath of a Large-Scaleflat-Subduction Event," in *The Evolution of the Chilean-Argentinean Andes*. Editor A. Folguera, et al. (Cham, Switzerland: Springe), 279–316.

Gleadow, A. J. W., and Duddy, I. R. (1981). A Natural Long-Term Track Annealing experiment for Apatite. *Nucl. Tracks Radiat. Measurements* 5 (1-2), 169–174. doi:10.1016/0191-278x(81)90039-1

Gleadow, A. J. W., Duddy, I. R., Green, P. F., and Lovering, J. F. (1986). Confined Fission Track Lengths in Apatite: A Diagnostic Tool for thermal History Analysis. *Contr. Mineral. Petrol.* 94 (4), 405–415. doi:10.1007/bf00376334

González, R., Wilke, G.-H., Riquelme, R., Menzies, A., Espinoza, F., and Herrera, C. (2015). Carta Sierra de Varas, Región de Antofagasta. Servicio Nacional de Geología y Minería, Carta Geológica de Chile. *Serie Geología Básica No.* 178 (1). 100.000.

Henriquez, S., DeCelles, P. G., and Carrapa, B. (2019). Cretaceous to middle Cenozoic exhumation history of the Cordillera de Domeyko and Salar de Atacama basin, northern Chile. *Tectonics* 38 (2), 395–416. doi:10.1029/2018TC005203

Horton, B. K. (2018). Tectonic Regimes of the central and Southern Andes: Responses to Variations in Plate Coupling during Subduction. *Tectonics* 37, 402–429. doi:10.1002/2017tc004624

Hurford, A. J., and Green, P. F. (1983). The Zeta Age Calibration of Fission-Track Dating. *Chem. Geology.* 41, 285–317. doi:10.1016/s0009-2541(83)80026-6

Jaillard, E., and Soler, P. (1996). Cretaceous to Early Paleogene Tectonic Evolution of the Northern Central Andes (0–18°S) and its Relations to Geodynamics. *Tectonophysics* 259 (1-3), 41–53. doi:10.1016/0040-1951(95)00107-7

Jordan, T. E., Muñoz, N., Hein, M., Lowenstein, T., Godfrey, L., and Yu, J. (2002). Active Faulting and Folding without Topographic Expression in an Evaporite basin, Chile. *Geol. Soc. Am. Bull.* 114 (11), 1406–1421. doi:10.1130/0016-7606(2002)114<1406:afafwt>2.0.co;2

Jordan, T., Mpodozis, C., Muñoz, N., Blanco, P., Pananont, M., and Gardeweg, M. (2007). Cenozoic subsurface stratigraphy and structure of the Salar de Atacama basin, northern Chile. *J. S. Am. Earth Sci.* 23 (2-3), 122–146. doi:10.1016/j.jsames.2006.09.024

Kay, S. M., Ramos, V. A., Mpodozis, C., and Sruoga, P. (1989). Late Paleozoic to Jurassic Silicic Magmatism at the Gondwana Margin: Analogy to the Middle Proterozoic in North America. *Geol* 17, 324–328. doi:10.1130/0091-7613(1989)017<0324:lptjsm>2.3.co;2

López, C., Martínez, F., Maksymowicz, A., Giambiagi, L., and Riquelme, R. (2019). What Is the Structure of the Forearc Region in the Central Andes of Northern Chile? an Approach from Field Data and 2-D Reflection Seismic Data. *Tectonophysics* 769, 228187. doi:10.1016/j.tecto.2019.228187

López, C., Riquelme, R., Martínez, F., Sánchez, C., and andMestre, A. (2017). Zircon U-Pb Geochronology of the Mesozoic to Lower Cenozoic Rocks of the Coastal Cordillera in the Antofagasta Region (22°30′–23°00′S): Insights to the Andean Tectono-Magmatic Evolution. *J. South. Am. Earth Sci.* 87, 113–138.

Maksaev, V., Munizaga, F., and Tassinari, C. (2014). Temporalidad del magmatismo del borde paleo-Pacífico de Gondwana: geocronología U-Pb de rocas ígneas del Paleozoico tardío a Mesozoico temprano de los Andes del norte de Chile entre los 20° y 31°S. *Andgeo* 41 (3), 447–506. doi:10.5027/andgeoV41n3-a01

Marinovic, N., Smoje, I., Maksaev, V., Herve, M., and Mpodozis, C. (1995). Hoja Aguas Blancas, región de Antofagasta. *Serv. Nac. Geol. Min. Doc. Trab.* 70.

Martínez, F., Arriagada, C., Peña, M., Deckart, K., and Charrier, R. (2016). Tectonic Styles and Crustal Shortening of the Central Andes "Pampean" Flat-Slab Segment in Northern Chile (27-29°S). *Tectonophysics* 667, 144–162. doi:10.1016/j.tecto.2015.11.019

Martínez, F., Kania, J., Muñoz, B., Riquelme, R., and López, C. (2020b). Geometry and Development of a Hybrid Thrust belt in an Inner Forearc Setting: Insights from the Potrerillos Belt in the Central Andes, Northern Chile. *J. South Am. Earth Sci.* 98, 102439. doi:10.1016/j.jsames.2019.102439

Martínez, F., López, C., Bascuñan, S., and Arriagada, C. (2018). Tectonic Interaction between Mesozoic to Cenozoic Extensional and Contractional Structures in the Preandean Depression (23°-25°S): Geologic Implications for the Central Andes. *Tectonophysics* 744, 333–349. doi:10.1016/j.tecto.2018.07.016

Martínez, F., López, C., and Parra, M. (2020a). Effects of pre-orogenic tectonic structures on the Cenozoic evolution of Andean deformed belts: Evidence from the Salar de Punta Negra Basin in the Central Andes of Northern Chile. *Basin Res.* 32 (6), 1441–1462. doi:10.1111/bre.12436

Martínez, F., López, C., Parra, M., and Espinoza, D. (2019). Testing the occurrence of thick-skinned triangle zones in the central Andes forearc: example from the salar de Punta Negra basin in northern Chile. *J. Struct. Geology.* 120, 14–28. doi:10.1016/j.jsg.2018.12.009

McClay, K., Dooley, T., and Whitehouse, P. (2002). 4-D Evolution of Rift Systems: Insights from Scaled Physical Models. *AAPG Bull.* 86 (6), 935–959. doi:10.1306/61eedbf2-173e-11d7-8645000102c1865d

McKenzie, D. (1978). Some Remarks on the Development of Sedimentary Basins. *Earth Planet. Sci. Lett.* 40 (1), 25–32. doi:10.1016/0012-821x(78)90071-7

Meesters, A. G. C. A., and Dunai, T. J. (2002). Solving the Production-Diffusion Equation for Finite Diffusion Domains of Various Shapes. Part I. Implications for Low-Temperature (U-Th)/He Thermochronology. *Chem. Geol.* 186 (3-4), 333–344. doi:10.1016/s0009-2541(01)00422-3

Mégard, F. (1978). ÉtudeGeologiquedes Andes duPérouCentral.Contribution a L'etudegeologiquedes Andes N°1. *Mémoire ORSTROM* 86, 310, 1978 . Paris.

Morandé, J., Gallardo, F., and Farías, M. (2015). Carta Guaviña, Región de Tarapacá. Servicio Nacional de Geología y Minería, Carta Geológica de Chile. *Serie Geología Básica* 177 (1). 100.000.

Mpodozis, C., and Ramos, V. A. (2008). Tectónica jurásica en Argentina y Chile: Extensión, Subducción Oblicua, Rifting, Deriva y Colisiones. *Rev. Geol. Argent.* 63, 479–495.

Mpodozis, C., Arriagada, C., Basso, M., Roperch, P., Cobbold, P., and Reich, M. (2005). Late Mesozoic to Paleogene stratigraphy of the Salar de Atacama Basin, Antofagasta, northern Chile: Implications for the tectonic evolution of the Cental Andes. *Tectonophysics* 399 (1–4), 125–154. doi:10.1016/j.tecto.2004.12.019

Mpodozis, C., and Kay, S. (1990). Provincias magmáticas ácidas y evolución tectónica de Gondwana: Andes chilenos (28-31°S). *Revista Geológica de Chile* 17 (2), 153–180.

Muñoz, N., Charrier, R., and Jordan, T. (2002). Interactions between basement and cover during the evolution of the Salar de Atacama basin, northern Chile. *Rev. Geol. Chile* 29, 55–80. doi:10.4067/s0716-02082002000100004

Niemeyer, H., Urzúa, F., and Rubinstein, C. (1997). Nuevos antecedentes estratigráficos y sedimentológicos de la Formación Zorritas, Devónico-Carbonífero de Sierra Almeida. Reg. Antofagasta, Chile. *Rev. Geol. Chile* 24 (1), 25–43.

Pananont, P., Mpodozis, C., Blanco, N., Jordan, T. E., and Brown, L. D. (2004). Cenozoic evolution of the northwestern Salar de Atacama Basin, northern Chile. *Tectonics* 23, a–n. doi:10.1029/2003TC001595

Ramos, V. A. (2009). "Anatomy and Global Context of the Andes: Main Geologic Features and the Andean Orogenic Cycle," in *Backbone of the Americas: Shallow Subduction, Plateau Uplift, and Ridge and Terrane Collision*. Editors , et al.(Washington: Geological Society of America Memoir 204), 31–65. doi:10.1130/2009.1204(02)

Reiners, P. W., and Brandon, M. T. (2006). Using Thermochronology to Understand Orogenic Erosion. *Annu. Rev. Earth Planet. Sci.* 34, 419–466. doi:10.1146/annurev.earth.34.031405.125202

Rubilar, J., Martínez, F., Arriagada, C., Becerra, J., and Bascuñán, S. (2017). Structure of the Cordillera de la Sal: A key tectonic element for the Oligocene-Neogene evolution of the Salar de Atacama basin, Central Andes, northern Chile. *J. South Am. Earth Sci.* 87, 200–210.

Rubinstein, C., Petus, E., and Niemeyer, H. (1997). Palynostratigraphy of the Zorritas Formation, Antofagasta Region, Chile: Insights on the Devonian/Carboniferous Boundary in Western Gondwana. *Geosci. Front.* 8 (3), 493–506.

Semperé, T., Butler, R. F., Richards, D. R., Marshall, L. G., Sharp, W., Swisher, C. C., et al. (1997). Stratigraphy and Chronology of Upper Cretaceous-Lower Paleogene Strata in Bolivia and Northwest Argentina. *Geol. Soc. América Bull.* 109 (6), 709 – 727. doi:10.1130/0016-7606(1997)109<0709:sacouc>2.3.co;2

Semperé, T., Carlier, G., Soler, P., Fornari, M., Carlotto, V., and andJacay, J. (2002). Late Permian-Middle Jurassic Lithospheric Thinning in Perú and Bolivia, and its Bearing on Andean-Age Tectonics. *Tectonophysics* 345 (1-4), 153–181. doi:10.1016/s0040-1951(01)00211-6

Sobel, E. R., and Seward, D. (2010). Influence of Etching Conditions on Apatite Fission-Track Etch Pit Diameter. *Chem. Geology.* 271 (1-2), 59–69. doi:10.1016/j.chemgeo.2009.12.012

Solari, M., Venegas, C., Montecino, D., Astudillo, N., Cortés, J., Bahamondes, B., et al. (2017). Geología del área Imilac-Quebrada Guanaqueros, Región de Antofagasta. Servicio Nacional de Geología y Minería, Carta Geológica de Chile. *Ser. Geol. Básic.* 191 (1). :100.000.

Soto, R., Martinod, J., Riquelme, R., Hérail, G., and Audin, L. (2005). Using Gemorphological Markers to Discriminate Neogene Tectonic Activity in the Precordillera of North Chilean Forearc (24-25°S). *Tectonophysics* 411, 41–55. doi:10.1016/j.tecto.2005.08.017

Steinman, G. (1929). *Geologie von Peru*. (Berlin: Carl Winters Universitats-Buchhandlung), 448.

Tankard, A. J., Uliana, M. A., Welsink, H. J., Ramos, V. A., Turic, M., Franca, A. B., et al. (1995). "Structural and Tectonic Controls of basin Evolution in Southwestern Gondwana during the Phanerozoic," in *Petroleum Basins of South America*. Editors , et al.(Tulsa: AAPG Memoir. 62. AAPG), 5–52. doi:10.1306/m62593c1

Wernicke, B. P. (1981). Low-angle normal Faults in the Basin and Range Province: Nappe Tectonics in an Extending Orogeny. *Geol. Soc.* Am13, 113–114.

Xiao, H., and Suppe, J. (1992). Origin of Rollover. *Am. Assoc. Pet. Geologists Bull.* 76, 509–229. doi:10.1306/bdff8ccc-1718-11d7-8645000102c1865d

Ziegler, P. A., and Cloetingh, S. (2004). Dynamic Processes Controlling Evolution of Rifted Basins. *Earth-Science Rev.* 64, 1–50. doi:10.1016/s0012-8252(03)00041-2

Conflict of Interest: The authors declare that the research was conducted in the absence of any commercial or financial relationships that could be construed as a potential conflict of interest.